AMERICAN UNIVERSITY OF BEIRUT

STIFFNESS MODELING OF BOLTED THICK BUILT-UP T-STUB CONNECTIONS INCLUDING SECONDARY PRYING EFFECT

by
NABIL HASSAN ABBOUD

A thesis
submitted in partial fulfillment of the requirements
for the degree of Master of Engineering
to the Department of Civil and Environmental Engineering
of the Faculty of Engineering and Architecture
at the American University of Beirut

Beirut, Lebanon
April 2014

AMERICAN UNIVERSITY OF BEIRUT

STIFFNESS MODELING OF BOLTED THICK BUILT-UP
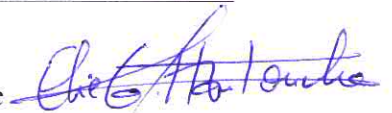T-STUB CONNECTIONS INCLUDING SECONDARY PRYING
EFFECT

by
NABIL HASSAN ABBOUD

Approved by:

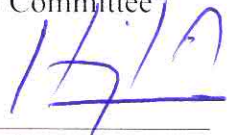|		
Dr. Elie Hantouche, PhD Civil and Environmental Engineering	Advisor Signature	
Dr. Muhammad Harajli, PhD Civil and Environmental Engineering	Member of Committee Signature	
Dr. Shadi Najjar, PhD Civil and Environmental Engineering	Member of Committee Signature	
Dr. George Saad, PhD Civil and Environmental Engineering	Member of Committee Signature	

Date of thesis/dissertation defense: April 28, 2014

THESIS, DISSERTATION, PROJECT RELEASE FORM

Student Name:

Abboud   Nabil   Hassan
_____   _____   _____
Last   First   Middle

● Master's Thesis   ○ Master's Project   ○ Doctoral
Dissertation

☒   I authorize the American University of Beirut to: (a) reproduce hard or electronic copies of my thesis, dissertation, or project; (b) include such copies in the archives and digital repositories of the University; and (c) make freely available such copies to third parties for research or educational purposes.

☐   I authorize the American University of Beirut, **three years after the date of submitting my thesis, dissertation, or project,** to: (a) reproduce hard or electronic copies of it; (b) include such copies in the archives and digital repositories of the University; and (c) make freely available such copies to third parties for research or educational purposes.

_____   12/05/2014
Signature   Date

ACKNOWLEDGMENTS

AN ABSTRACT OF THE THESIS OF

Nabil Hassan Abboud   for   Master of Engineering
                              Major: Civil and Environmental Engineering

Title: stiffness modeling of bolted thick built-up T-stub connections including secondary prying effect

The main goal of this research is to predict the behavior of T-stub connections associated with deep beams, including column deformations, which meet the prequalification requirements for moment resisting frames (MRF). The results of experimental tests and finite element (FE) simulations are used to develop a stiffness model that predicts the behavior of bolted thick built-up T-stub connections including column flange deformation, and accounting for primary and secondary prying effect. The model incorporates the overall T-stub and column flange deformations of key component elements, and includes nonlinear material behavior of bolts and base material, and accounts for pretension of fasteners and contact interaction. The stiffness model consists of linear and nonlinear springs which model deformations from tension bolt elongation, slip-bearing, bending of T-stub flange, elongation of the T-stem, column flange deformation, and accounts for primary and secondary prying forces. The behavioral characteristics of the T-stub/column flange system are examined including strength, stiffness, deformation, and energy dissipation. A proposed strength model that predicts the capacity of the column flange for the failure mode of full plastification at the flange-to-web connection of the column (K-zone) followed by interior tension bolt fracture is developed. Furthermore, closed form expressions that are based on stiffness modeling techniques are developed to predict the energy dissipation capacity of the T-stub/column flange system with and without continuity plates. Comparison of the models predictions with experimental and FE data shows that the proposed models accurately predict the connection and the column flange load-deformation response. This research provides guidelines for engineers to account for the additional forces induced in the tension bolts and for the maximum rotational capacity demand in the connection which are required for seismic analysis and design.

CONTENTS

Appendix

ILLUSTRATIONS

TABLES

ABBREVIATIONS

ε_y: yield strain for the base material

ΔT: change in temperature

B_0: minimum bolt pretension force as specified in the ANSI/AISC 360-10

A_b: nominal gross area of the bolt

α: coefficient of thermal expansion

E: Young's modulus of elasticity

L_{sb}: effective T-stem length contributing to the deformation

L_{st}: total length of the T-stem

t_s: thickness of the T-stem

$K_{e,stem}$: elastic stiffness of the T-stem

W_{stem}: width of the T-stem

E: elastic modulus of the base material

$P_{y,stem}$: yield load of the T-stem

F_y: yield stress of the base material

d_h: hole diameter

$K_{p,stem}$: plastic T-stem stiffness

L_e: edge distance

g_s: vertical gage distance between successive rows of shear bolts

E_s: tangent modulus of elasticity

$P_{u,stem}$: ultimate load of the T-stem

F_u: ultimate stress of the material

B: current force in the tension bolt

B_0: minimum pretension force per bolt as specified by ANSI/AISC 360

B_n: tensile capacity of the bolt

$B_{fracture}$: fracture load of the bolt

K_b: stiffness of the bolt in the elastic range

T: applied force in the column flange model

Δ: vertical displacement of the K-zone in the column flange

d_b: bolt diameter

$k_{eee,kk}$: stiffness of the column flange when it is still in its elastic range with both tension bolts in the kth stiffness state

$k_{pee,kk}$: stiffness of the column flange when plastification has occurred at the K-zone and both tension bolts are in the kth stiffness state

ΔB_{int}: change in the interior bolt force

ΔB_{ext}: change in the exterior bolt force

$\Delta M_{K\text{-}zone}$: change in the moment at the K-zone

ΔQ: prying gradient

ΔT: change in the applied load

a: length of a column flange measured from the inside edge of the exterior bolt line to the outside edge of the column flange

b: gage distance between the tension bolts

c: length of the column flange measured from the inside edge of the interior bolt to the location of occurrence of the plastic hinge at the K-zone of the column flange

γ_1: constants used in the calculation of the column flange stiffness

γ_2: constants used in the calculation of the column flange stiffness

γ_3: constants used in the calculation of the column flange stiffness

γ_4: constants used in the calculation of the column flange stiffness

γ_5: constants used in the calculation of the column flange stiffness

γ_6: constants used in the calculation of the column flange stiffness

γ_7: constants used in the calculation of the column flange stiffness

γ_8: constants used in the calculation of the column flange stiffness

γ_9: constants used in the calculation of the column flange stiffness

γ_{10}: constants used in the calculation of the column flange stiffness

γ_{11}: constants used in the calculation of the column flange stiffness

γ_{12}: constants used in the calculation of the column flange stiffness

γ_{13}: constants used in the calculation of the column flange stiffness

γ_{14}: constants used in the calculation of the column flange stiffness

γ_{15}: constants used in the calculation of the column flange stiffness

γ_{16}: constants used in the calculation of the column flange stiffness

A: the cross sectional area

f_s: shape factor used in computing the shear deformations

G: shear modulus of elasticity

I: second moment of inertia of a cross section

$K_{b1,k}$: stiffness of the interior bolt in the kth range

$K_{b2,k}$: stiffness of the exterior bolt in the kth range

p: tributary area per bolt

t_{cf}: thickness of the column flange

t_{Tf}: thickness of the T-stub flange

$K_{cp,eee}$: elastic stiffness of the column flange including continuity plates

B_{1n}: tensile capacity of the exterior tension bolt

B_{2n}: the tensile capacity of the interior tension bolt

M_p: plastic moment capacity

E_D: energy dissipation capacity of the T-stub

P_u: ultimate load of the T-stub

$P_{y,flange}$: yield load of the T-flange

t_{Tf}: thickness of the T-flange

θ_u: rotation of the flange at which bolt fracture occurs

θ_c: rotation of the flange at which stem fracture occurs

θ_y: rotation of the flange at which partial yielding of the T-flange occurs

ε_y: strain at yielding of the steel

P_{slip}: load that causes relative slip between the beam flange and the T-stem

Δ_{slip}: relative slip between the beam flange and the T-stem which is equal to the hole clearance

L: moment arm for the T-flange stiffness model

$K_{e,flange}$: initial stiffness of the T-flange stiffness model

$K_{bearing}$: bearing stiffness of the slip and bearing stiffness model

λ_1: constants used for the calculation of the energy dissipation capacity of the T-stub

λ_2: constants used for the calculation of the energy dissipation capacity of the T-stub

λ_3: constants used for the calculation of the energy dissipation capacity of the T-stub

CHAPTER I

INTRODUCTION & LITERATURE REVIEW

A. Introduction

T-stub connections are considered to be one of the stiffest types of connections, as shown in Fig. 1 and may be described as rigid connections. Characterizing the behavior of T-stub connections requires complete knowledge about its strength, stiffness, and ductility.
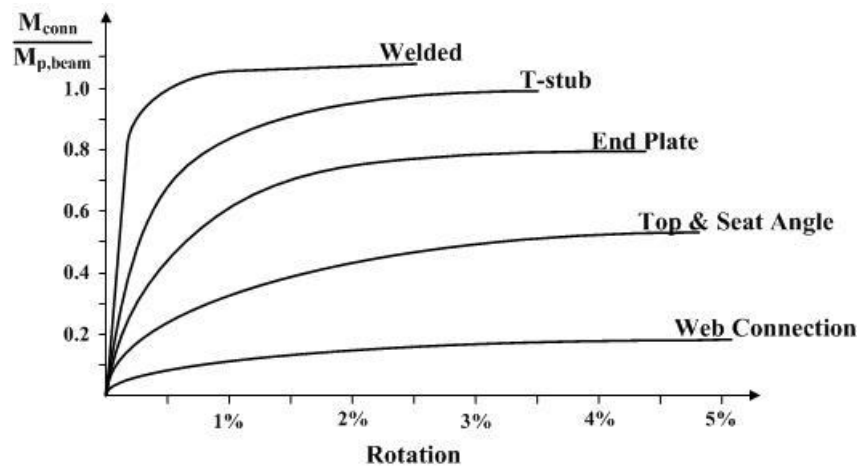
Fig. 1 – Moment rotation characteristics of typical connections (AISC Specs 2005).

Previous research work on the behavior of T-stub connections dealt with estimating the strength, stiffness, and deformation using experimental investigation [1–6], finite element simulations (FE) [2,3,6–9], and stiffness and strength modeling [8,10–16] including primary prying effect and assuming rigid column flange.

The accuracy of the above analytical models was demonstrated to be acceptable by comparing the results predicted with experimental results. Continuity plates in columns are often used in connections to stiffen the column flange and web in order to resist large forces transmitted by the beam flange. It was reported that column flange bending displacements were relatively small compared to those of T-stub flange when continuity plates were provided. Also, the column flange deformation was considered negligible when column flange thickness is larger than that of T-stub flange [8]. However, for thick flange T-stub connections that are connected to a thinner column flange, the deformation from the column side is significant when continuity plates are not provided. In such cases, the column flange is subjected to bending, and may undergo significant deformations. This behavioral characteristic of the column flange causes the secondary prying phenomenon as shown in Fig. 2(a). Secondary prying refers to the additional forces introduced in the tension bolts due to bending of the column flange [8]. Fig. 2(b) shows a typical design sketch for a built-up T-stub connection associated with deep girders.

Column side

g_c

t_{cf}

t_{Tf}

T-stub side

(b)

¾" Continuity plates 4 places

8, 1 1/8" A490

16, 7/8" A490-X

5, 1" A490-X

W24x76

W14x257
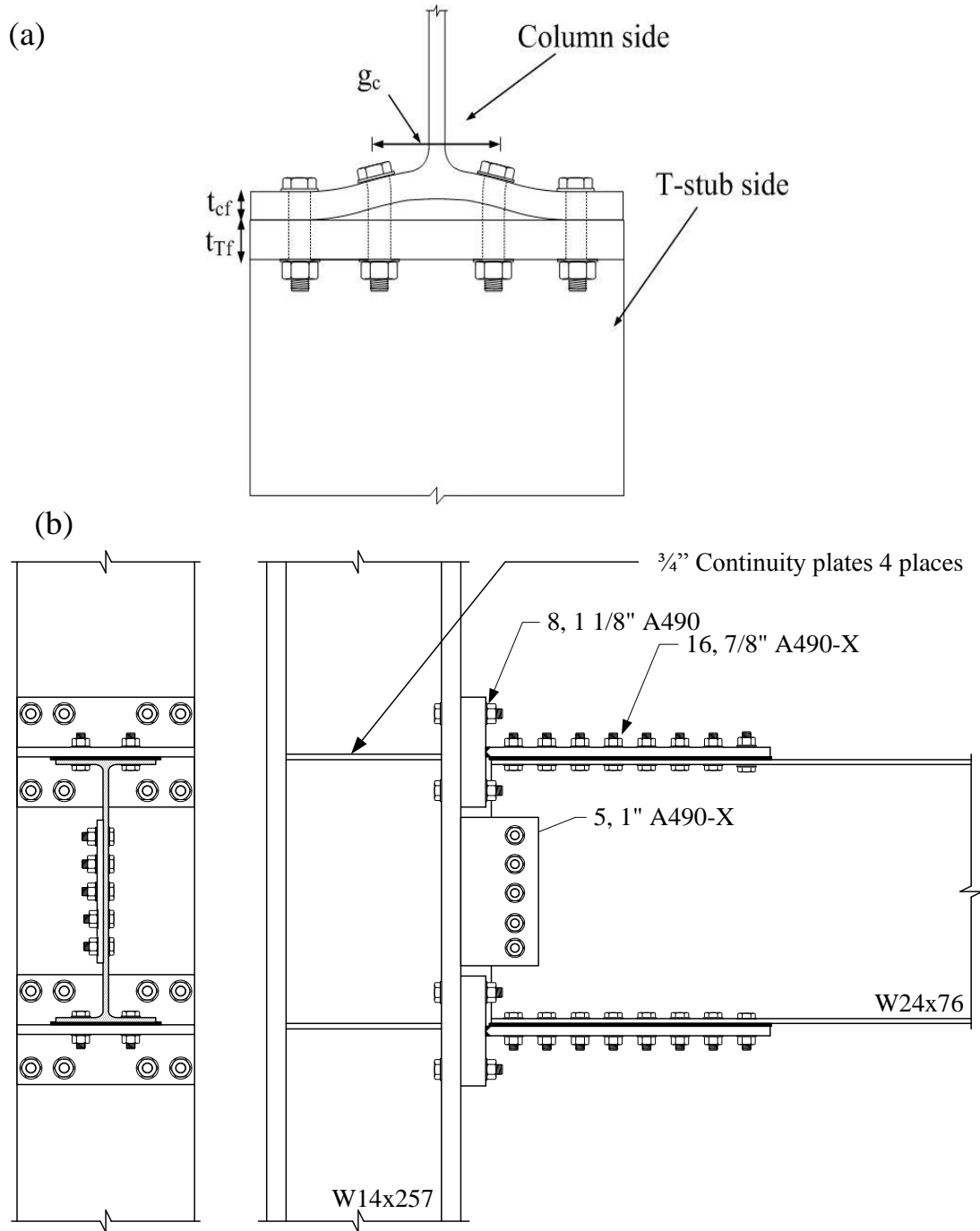
Fig. 2 – (a) Top view of the T-stub/column flange system, (b) Design sketch for a typical built-up T-stub connection associated with W24x76 beam.

Investigation of the secondary prying effect in thick built-up T-stub connections has been developed to predict only its strength and did not account for its stiffness and ductility [8]. Therefore, a stiffness model of the T-stub/column flange system that takes into account the effect of secondary prying is needed to predict the force-deformation response. The existing T-stem model available in the literature [11-12,15] is based on broad assumptions regarding the stress concentrations around the shear bolts and does not account for the contribution of the stresses outside the bolt gage area when dealing with thick built-up T-stubs where wide stems are supplied. Therefore, a modification of existing models is needed to accurately predict the response of wide T-stems associated with deep girders.

In this research, a proposed model based on stiffness approach is developed to predict the built-up T-stub response including the column flange deformation with and without continuity plates. With its simplicity in application when compared to other numerical methods (i.e. FE analysis), the proposed model is capable of accounting for primary and secondary prying; and allows the prediction of tension bolt elongation, bending deformation of the T-stub flange, bearing deformation of the T-stem, and column flange deformation with and without continuity plates. These ultimate deformation predictions can be used to calculate the maximum rotational capacity of thick T-stub connection including column flange. Furthermore, a column flange strength model that predicts the capacity of full plastification at the flange-to-web connection of the column (K-zone) followed by interior tension bolt fracture is developed. Also, closed form equations are proposed to predict the energy dissipation of thick flange T-stub

4

connections/column flange system including the secondary prying effect. In addition to the above contributions, this research also provides a simplified and rational method for theoretically predicting the strength, stiffness, and ductility of T-stub connections including column flange bending and its effect on the connection behavior. The stiffness models developed in this research were validated against the results of an experimental program carried out earlier by Hantouche et al. [2].

B. Literature review

Several researchers have attempted to characterize the behavior of T-stub connections without considering the contribution from the column flange.

1. Hu et al. (2011) slip and bearing model

Hu et al. [11] proposed a stiffness model to characterize the behavior of the slip and bearing mechanism in T-stub connections. Slip limits the stresses transformed from the shear bolts to the plates and contribute to significant energy dissipation. Slip arises from the direct shear forces on the slip planes that are originated from the axial tensile force on the connection. Once the slip force exceeds the slip resistance, slip will occur between the two surfaces in contact. Hu et al. [11] proposed the following equation to predict the slip resistance:

$$P_{slip} = 1.13 \mu h_{sc} T_b n_s n_{sc} \tag{1}$$

where μ is the friction coefficient depending on the surfaces in contact, h_{sc} is the coefficient for the standard bolt holes, T_b is the minimum pretension force in the bolt as

5

specified by AISC Specs, n_s is the number of shear planes, and n_{sb} is the number of shear bolts.

The slip plateau corresponds to the construction clearance, Δ_c. In their model, Hu et al. [11] assumed that the slip occurs with some resistance, and thus the slip stiffness, $K_{i,slip}$, was defined as 1% of the initial stiffness, where the initial stiffness corresponds to the pre-slip stiffness. The initial stiffness can be calculated as proposed by Hu et al. [11] by determining the slip load from eq. (1) above and the pre-slip displacement, Δ_p. The pre-slip displacement was defined as 0.2 mm, where the value of 0.2 was used as recommended by Rex and Esterling. Thus, the initial stiffness can be calculated as follows:

$$K_{i,slip} = \frac{P_{slip}}{\Delta_p} \tag{2}$$

After, the slip occurs, the shear bolts starts to bear against the plates (beam flange and T-stem), and the stiffness picks up again. Hu et al. [11] proposed the following equation to predict the bearing stiffness, $K_{e,bearing}$:

$$K_{e,bearing} = K_{br} \tag{3}$$

where K_{br} corresponds to the bolt bearing stiffness and can be computed as follows as proposed by Hu et al. [11]:

$$K_{br} = 120 F_y t_w d_b^{0.8} \tag{4}$$

where F_y corresponds to the yield stress of the base material, t_w corresponds to the thickness of the plate on which the bolts are bearing, and d_b correspond to the bolt diameter.

2. Swanson and Leon (2001) T-stem model

Swanson and Leon [15] proposed a bilinear stiffness model to predict the behavior of the T-stem. The model consists on defining 4 parameters corresponding to the initial T-stem stiffness, $K_{e,stem}$, the tangent stiffness of the T-stem, $K_{p,stem}$, the yield load, $F_{y,stem}$, and the ultimate deformation of the T-stem, $\Delta_{u,stem}$. To compute the initial stiffness of the T-stem a tapered beam model was assumed. The width of the end of the tapered beam model was set equal to the flange width of the connected beam, and the angle of inclination of the tapered edges relative to the axis of the beam was limited to a value no greater than 30° based on a research conducted by Whitmore (1952). Material excluded by this angle was not considered to contribute to the stiffness of the T-stem. The stresses were assumed to be distributed uniformly along the length of the tapered length of the T-stem. Thus, the elastic stiffness proposed by Swanson and Leon [15] can be calculated as follows:

$$K_{e,stem} = \frac{4L_{sb}t_sE(\tan\theta)^2}{2L_{sb}\tan\theta + g_s \, ln\left(\dfrac{g_s}{2L_{sb}\tan\theta + g_s}\right)} \tag{5}$$

where L_{sb} is the distance from the first pair of shear bolts to the last pair, t_s is the thickness of the T-stem, E is the elastic modulus of elasticity of the T-stem, θ is the effective angle, and g_s is the gauge between two rows of shear bolts.

The plastic stiffness definition proposed by Swanson and Leon [15] was based on the assumption that the steel material between the last two bolt holes (nearest to the T-flange) starts to strain-harden before the rest of the cross section. Thus, the plastic stiffness can be calculated as follows:

7

$$K_{p,stem} = \frac{\left(g_s - d_{h,eff}\right)t_s E_s}{3d_b}$$

(6)

where $d_{h,eff}$ is the effective bolt hole diameter, d_b is the bolt diameter, and E_s is the tangent modulus of elasticity of the base material.

The yield load of the T-stem proposed by Swanson and Leon [15] was based on the assumption that the stress distribution in the T-stem cross section is uniform. Although this assumption does not reflect the true complexity of the stress distribution in the T-stem, it gave good results when compared to experimental results. The yield load can be calculated as follows:

$$P_{y,stem} = F_y \left(W_{eff} - 2d_{h,eff}\right)t_s$$

(7)

The ultimate deformation of the T-stem as defined by Swanson and Leon [15] was based on the assumption that the initial fracture in the T-stem initiates in the material between the last two bolt rows. Thus, the ultimate deformation can be defined as the sum of the plastic deformation in the material in this region and the elastic deformation of the rest of the material of the T-stem. The following equation defines the ultimate deformation as proposed by Swanson and Leon [15]:

$$\Delta_{u,stem} = \varepsilon_{fract} d_{h,eff} + \frac{P_{y,stem}}{K_{e,stem}}$$

(8)

where ε_{fract} corresponds to the strain at fracture of the steel.

3. Hantouche et al. (2013) T-flange model

Hantouche et al. [10] developed a model to predict the behavior of built-up thick-flange in T-stub connections with Complete Joint Penetration (CJP) and fillet welds. The model is based on a combination of finite element and stiffness modeling approach that includes deformation of key components. The model also accounts for the nonlinear behavior of the base material (using a rotational spring) and the tension bolts (using a multi linear force-deformation curve to model their behavior). In addition, the model incorporates the pretension of the tension bolts and the contact between the T-flange and column flange (prying). The model predicts partial yielding at the K-zone of the T-flange followed by tension bolt fracture. The model also predicts the contact force between the T-flange and the column flange, the onset of yielding of the T-flange and the partial yielding penetration into the flange thickness as the external tensile load on the connection increases.

CHAPTER II

COMPONENT FINITE ELEMENT MODELING

FE analyses are conducted to better understand the behavior of the column flange and to provide data for validation of the proposed column flange model. The FE models include the column, the T-stub, part of the beam flange, and the tension and shear bolts. All components are modeled as three dimensional (3D) solid elements available within the software package ABAQUS [17]. The FE analyses conducted consider geometric and material nonlinearity, pretensioning of bolts, and contact interactions between element surfaces.

A. Three-dimensional solid (3D) FE model components modeling

In the FE models, continuum three-dimensional 20 nodes reduced integration element are used (C3D20-R) for all components as shown in Fig. 3. The model includes the column, T-stem, T-flange, 8 tension bolts, 18 shear bolts, and a plate representing the beam flange. The welds are not explicitly modeled but rather the tie constraint option between the welded surfaces is used in ABAQUS. The tie constraint option in ABAQUS allows the fusing of the two surfaces that are in contact even if the mesh on both surfaces is different. The interactions between the different parts are modeled using the finite sliding with a coefficient of friction of 0.25.
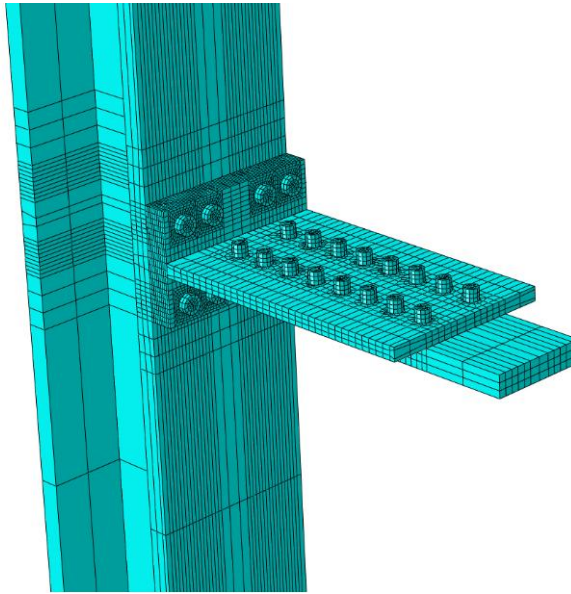
Fig. 3 – Discretization of the model assembly using C3D20-R elements.

B. Material properties

The Von Mises yield criterion is used in this research to define the onset of yielding. A bilinear stress-strain model with isotropic hardening is used to model the behavior of the bolts and the base material. For the bolt material, the yield and ultimate stress are taken as 117.53 kips (811 MPa) and 126.50 ksi (872 MPa), respectively. In addition, the yield and ultimate strain are taken as 0.00405 and 0.03084, respectively. Note that the values of the stress and strain are selected based on tensile coupon tests conducted on structural steel specimens [2]. In the FE models the bolts 'threads are not modeled but instead the gross area is used. For the base material, A572 Gr. 50 steel is used. According to the 2006 AISC seismic design manual [18], the values of the minimum specified tensile yield and ultimate stress can be increases by 10%. Thus, the values for the yield and ultimate tensile stress, corresponding to A572 Gr. 50 steel, used in this

11

research are 55.00 ksi (385 MPa) and 71.50 ksi (500 MPa), respectively. The yield strain

used for the base material is 0.00189, and the plastic strain is 0.09827 (50 ε_y). For all parts,

Young's modulus is assumed as 29000 ksi (203000 MPa) and poisson's ratio is taken as

0.30.

C. Boundary conditions

Boundary conditions are applied to the model throughout the analysis as shown in

Fig. 4. In the pretension step, the nodes on the top surface of the shear and tension bolts'

heads in addition the nodes on the surface of the T-flange are restrained against translation.

This is done to ensure contact between the bolts and plates during the analysis. The top

and bottom cross section of the column are also restrained against any translation and

rotation. In the loading step, all boundary conditions applied to the bolts and the T-flange

are deactivated. The boundary conditions on the top and bottom cross section of the

column are kept activated.

Column End Fixed

Tension
bolts
restrained
against
translation
in pretension
step

Surface
traction
applied to
the surface
of the plate

Shear bolts
restrained
against
translation
in pretension
step

Column End Fixed
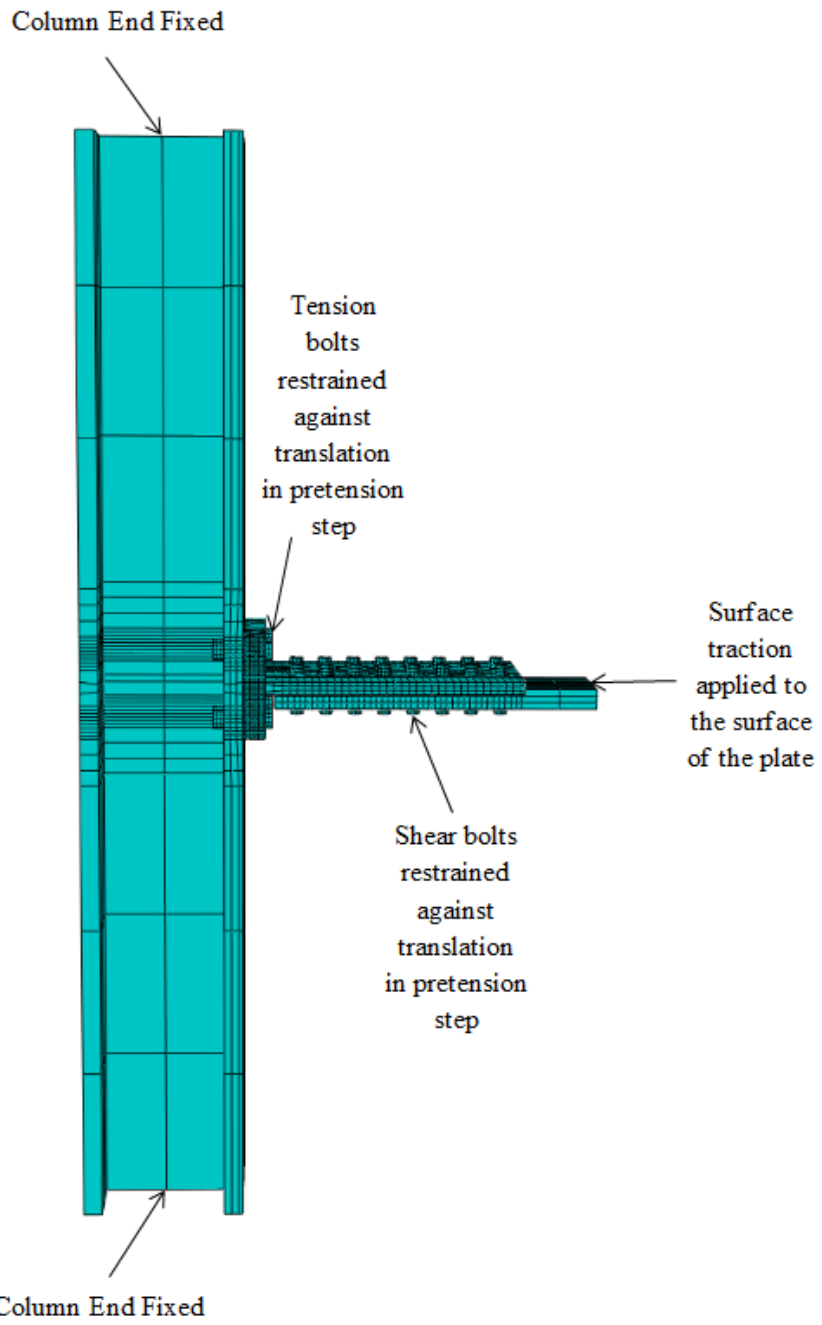
Fig. 4 – Boundary conditions applied on the model.

D. Loading

The loads are applied on the model in two steps. During the pretension step, the loads are pretentioned by applying a temperature change to the restrained bolt shank equivalent to the minimum specified pretension force in the AISC specifications. The temperature change required for the corresponding bolt diameter is obtained as follows:

$$\Delta T = \frac{B_0}{EA_b \alpha} \tag{9}$$

where B_0 (kips or kN) is the minimum bolt pretension force as specified in the ANSI/AISC 360-10, A (in^2 or cm^2) is the nominal gross area of the bolt, α (in./in.$^\circ$C) is the coefficient of thermal expansion, and E (ksi or MPa) is the Young's modulus of elasticity. By applying a negative temperature change the bolts' head and nut will come into contact with the T-stub and column flange. During the loading step, a tensile axial load is applied to the structure by applying a surface traction force to the beam flange as shown in Fig. 4. The Newton-Raphson method is used in the analysis.

CHAPTER III

STIFFNESS MODELING

In this research, the mechanisms that influence the behavior of thick built up T-stub connection are accounted for. These include tension bolt elongation, bending of T-stub flange, elongation of the T-stem, relative slip of the T-stub, bearing deformation of the T-stem, and column flange deformation including primary and secondary prying effect. Modeling the T-stub behavior is complex because all of these mechanisms interact with one another and hence simple strength checks cannot provide the necessary stiffness, ductility, and energy dissipation information that is required for seismic design.

A. Proposed T-stem stiffness model

Modeling the behavior of the T-stem is complex due to the non-uniform distribution of stresses along its cross section and its length, the interaction between the T-stem and the shear bolts, and the friction forces between the beam flange and the T-stem. The bilinear stiffness model developed by Swanson and Leon [15] showed disagreement when comparing with experimental and the FE results [2, 8]. This disagreement is due to the fact that the model does not account for the contribution of the stresses whenever yielding occurs along the full cross-section area. FE studies carried out in this research on thick built-up T-stubs, for thickness of the T-stem ranging from ½ in. (1-1/4 cm) to 2 in. (5 cm), showed that the main contribution of the deformation along the length of the T-stem is a function of the thickness of the T-stem as shown in Figs. 5(a) and 5(b). From the FE

results, the following equation is developed for describing the relationship between the effective T-stem length contributing to the deformation and the thickness of the T-stem with a linear fit of $R^2 = 0.99$:

$$\frac{L_{sb}}{L_{st}} = \begin{cases} -0.5661t_s + 1.3615 & (US \quad units) \\ -0.2228t_s + 1.3615 & (SI \quad units) \end{cases} \tag{10}$$

where L_{sb}(in. or cm) is the effective T-stem length contributing to the deformation, L_{st} (in. or cm) is the total length of the T-stem, and t_s(in. or cm) is the thickness of the T-stem.

Note that the above equations are derived based on a regression analysis including 5 data points that cover the range of stem thickness between ½ in. (1-1/4 cm) to 2 in. (5 cm). Grade 50 steel was assumed when deriving the above equations.

Eq. (10) was incorporated into the stiffness model developed in this research for predicting the behavior of the T-stem.
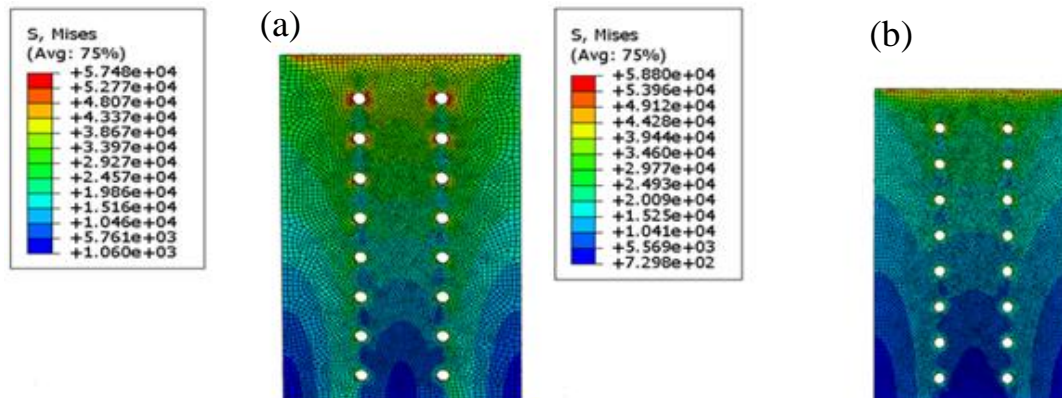
Fig. 5 – (a) von Mises stress contours along the cross section and length of the T-stem for a 1 in. thick T-stem, (b) von Mises stress contours along the cross section and length of the T-stem for a 1-1/2 in. thick T-stem.

16

1. Elastic stiffness

In this research, unlike the model developed by Swanson and Leon [15] where only part of the cross-section of the T-stem was considered effective, the total stem cross-section was assumed to contribute to its stiffness, ductility and strength. This assumption is consistent with the FE results performed in this research where the von Mises stresses were found to propagate to the outer edges of the T-stem and along the full cross-section as shown in Figs. 5(a) and 5(b). During the elastic range, the load is assumed to be uniformly distributed along the width of the T-stem, and therefore the elastic stiffness of the T-stem, $K_{e,stem}$, can be written as follows:

$$K_{e,stem} = \frac{W_{stem} t_s E}{L_{sb}} \tag{11}$$

where W_{stem} (in. or cm) is the width of the T-stem, and E (ksi or MPa) is the elastic modulus of the base material.

2. Yield load

The yield load, $P_{y,stem}$, is calculated by multiplying the cross section net area by the material yield stress as given by the equation below:

$$P_{y,stem} = F_y \left(W_{stem} - 2d_h \right) t_s \tag{12}$$

where F_y (ksi or MPa) is the yield stress of the base material and d_h (in. or cm) is the hole diameter.

Note that when deriving the above relationship, the T-stem is assumed to be subjected only to axial load, and that its behavior can be represented by a bar element.

17

3. Plastic stiffness

The plastic stiffness is calculated based on the assumption that the material, extending from the first to the nth row of bolts and around the bolt holes (Figs. 5(a) and 5(b)), starts to strain-harden before the remaining part of the cross section which is mainly dependent on the thickness of the T-stem, t_s. The plastic T-stem stiffness, $K_{p,stem}$, can be written as follows:

$$K_{p,stem} = \frac{\left(0.5L_e + g_s - d_h\right)t_s E_s}{L_{sb}} \tag{13}$$

where L_e (in. or cm) is defined as the edge distance, and the factor 0.5 is a constant representing the contribution of stresses outside the gage distance where the value was obtained from FE investigation, g_s (in. or cm) is the vertical gage distance between successive rows of shear bolts, and E_s (ksi or MPa) is the tangent modulus of elasticity.

4. Ultimate Load

The ultimate load of the T-stem, $P_{u,stem}$, was calculated by assuming a uniform stress distribution along the cross section of the T-stem in accordance with Hu et al. [11] and Swanson and Leon [15]. The ultimate load was calculated by multiplying the net cross sectional area by the material ultimate stress. The following equation is used to calculate the ultimate load at failure:

$$P_{u,stem} = F_u \left(W_{stem} - 2d_{h,eff}\right)t_s \tag{14}$$

where F_u (ksi or MPa) is the ultimate stress of the material.

5. Results

The accuracy of the proposed stiffness model of the T-stem described above is validated by comparing the model predictions against experimental results generated by Hantouche et al. [2] and the predictions of other existing models available in the literature [11-12, 15]. This is shown in the total force-deformation response of a ¾ in. (1.9 cm) thick T-stem depicted in Fig. 6(a). It can be seen from the results presented in Fig. 6(a) that the proposed stiffness model predicts experimental results considerably better than existing models (Swanson and Leon [15]). The stiffness T-stem model predicted an ultimate load capacity in the T-stem of 278 kips (1234 kN) and ultimate deformation capacity of 0.6 in. (1.48 cm) which are only 1% and 5% different from the experimentally measured ultimate load and deformation capacities of 281 kips (1250 kN) and 0.62 in. (1.55 cm), respectively.

In addition, the proposed stiffness model is compared to the total-force deformation response of a 1 ¼ in. (3.2 cm) thick T-stem as shown in Fig. 6(b). It can be seen that the proposed model can predict with good agreement the ultimate deformation and ultimate load of the T-stem. The stiffness T-stem model predicted an ultimate load capacity in the T-stem of 375 kips (1668 kN) and ultimate deformation capacity of 0.0542 in. (0.13 cm) which are only 4.5% and 3.5% different from the experimentally measured ultimate load and deformation capacities of 391 kips (1739 kN) and 0.0524 in. (0.13 cm), respectively.
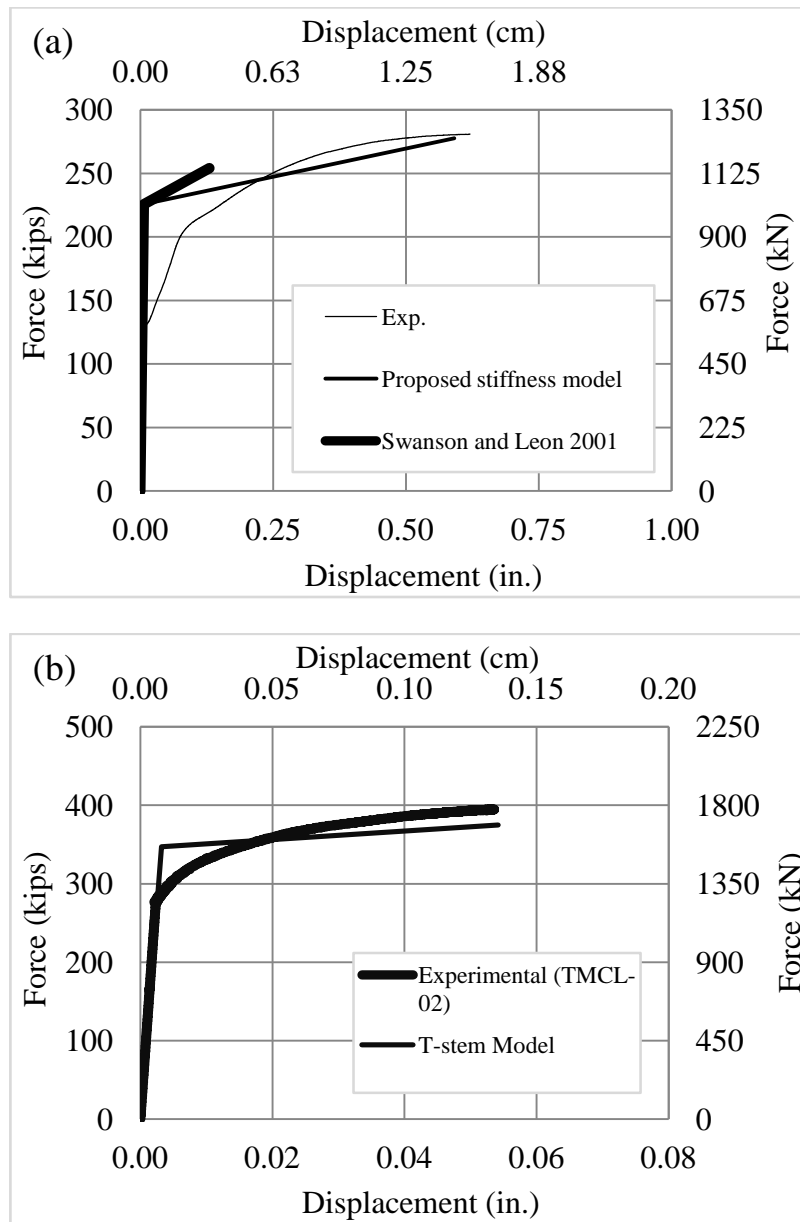
Fig. 6 – (a) Proposed T-stem stiffness model versus experimental and FE results (3/4 in. stem thickness) [2], (b) Comparison of the experimental results with the proposed modified T-stem model (TMCL-02).

The proposed stiffness is also compared to the FE results performed by Hantouche et al. (2012) [8] for thick built-up T-stub associated with deep girders (W24x76 and W30x108) and the results are presented in Figs. 7(a) and 7(b). It can be seen that the

proposed stiffness model can predict with reasonable agreement the initial stiffness of the

T-stem. Note that for those cases yielding of the T-stem did not occur before failure of the

connection.
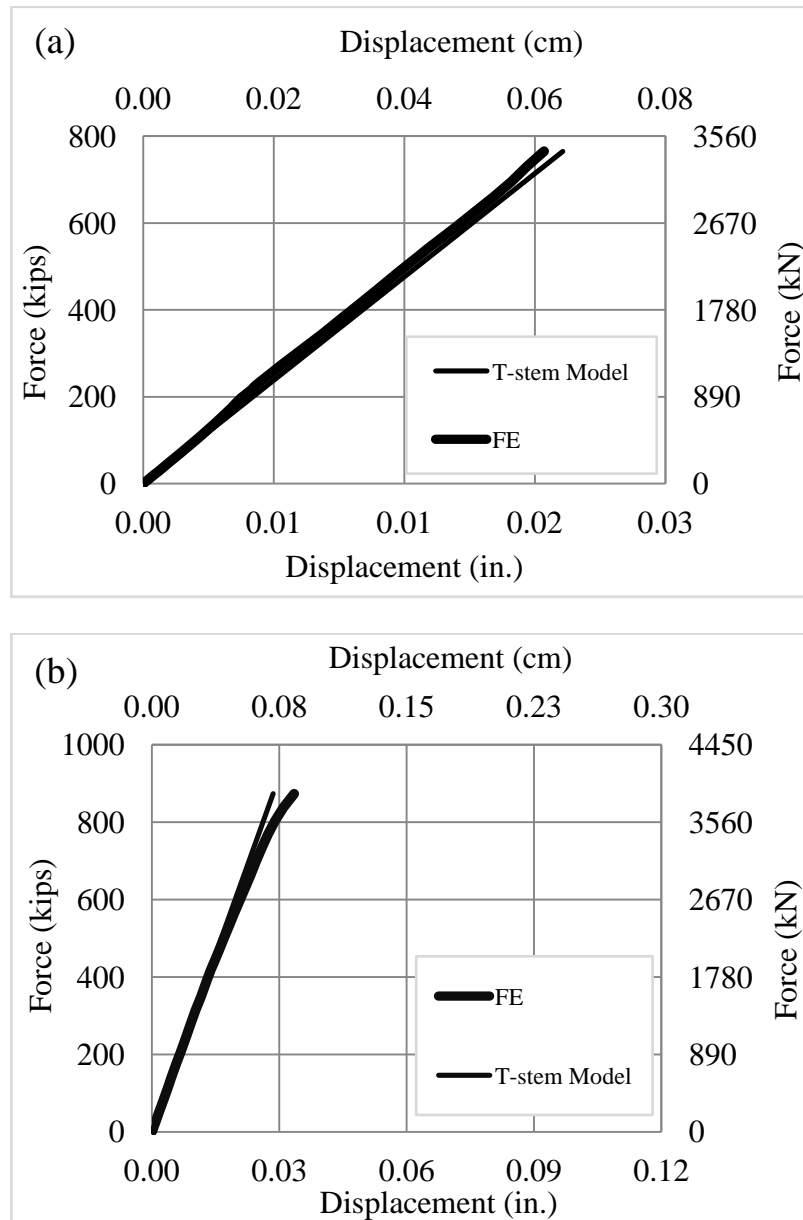
Fig. 7- Comparison of the finite element results with the proposed modified T-stem model
associated with, (a) W24x76 beam**,** (b) W30x108 beam.

B. Thick flange T-stub/tension bolt stiffness model

In this research, the existing stiffness model developed by Hantouche et al. [10] is used to determine the force-deformation response for thick flange T-stub connections. The model is composed of a bolt model and a flange model, and is able to predict partial yielding of the flange at the K-zone followed by bolt fracture. The model uses geometrical and mechanical properties consistent with previous stiffness models that are based on incremental analysis [12-15]. Nonlinear material behavior is accounted for in this formulation. A multi-linear force-deformation model is used for the bolts to idealize the behavior obtained from tensile test conducted for the bolts [10]. The partial yielding in the thick T-flange is accounted for by incorporating a nonlinear torsion spring at the K-zone. The bolt model incorporates a variable bolt stiffness that captures the changing behavior of the bolts as a function of the load that they are subjected to.

1. Results

The performance of the stiffness model for a thick built-up T-stub flange was validated by comparing the model prediction with experimental and FE results. The model [10] was found to accurately predict the force-deformation response taking into account bolt pretensionning, partial yielding of the flange, and contact phenomena as shown in Fig. 8.
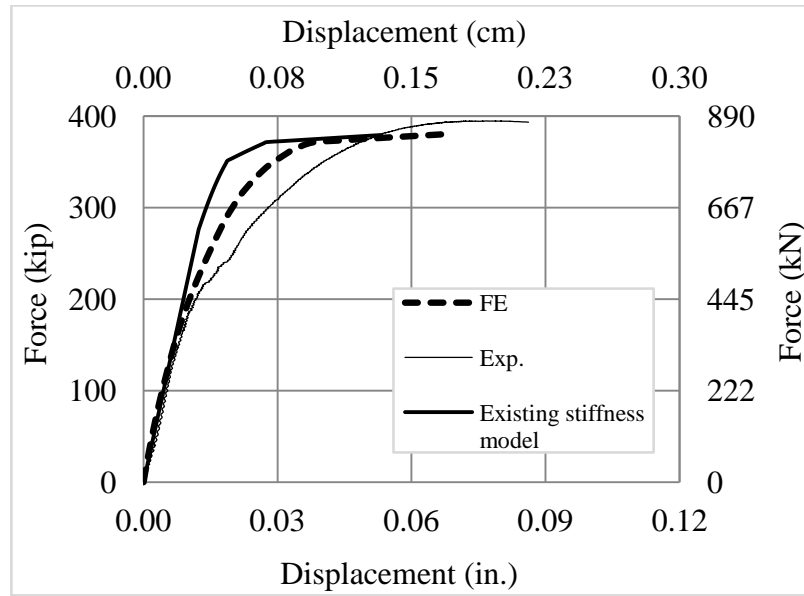
Fig. 8 – Existing T-flange stiffness model versus experimental and FE results [10].

C. Slip and bearing stiffness model

The existing stiffness model developed by Hu et al. [11] is used to reproduce the force-deformation response of the slip and bearing mechanism. The model combines the bearing deformation of the T-stem, and the relative slip between the T-stem and the beam flange. The model predicts first deformation from the T-stem until the applied load reaches the slip load. At the onset of the slip load, relative slip between the beam flange and the T-stem occurs leading to a significant loss of stiffness. As the load increases beyond the slip load the shear bolts start to bear against the beam flange and thus the stiffness increases again. Loading continues until yielding of the T-stem. Finally, at a certain load level beyond yielding, net section fracture of the T-stem occurs.

1. Results

The slip and bearing stiffness model is validated by comparison with FE results

performed by Hantouche et al. [8] for thick built-up T-stub connections associated with

W30x108 beam as shown in Fig. 9. It is shown that the model accurately predicts the

force-deformation curve for the slip and bearing. Note that the slight difference in the slip

plateau between the existing model and the FE results is due to stress concentrations that

occurred around the bolt holes in the FE analysis which are not considered in the existing

model. In other words, due to the holes, the region around the bolt holes will feel much

higher stresses which will results in additional deformations around the bolt hole. This

complex distribution of the stresses is captured by the FE model but is not considered by

the stiffness model since it is assumed that the stresses in the T-stem are uniform on the

cross section of the T-stem.
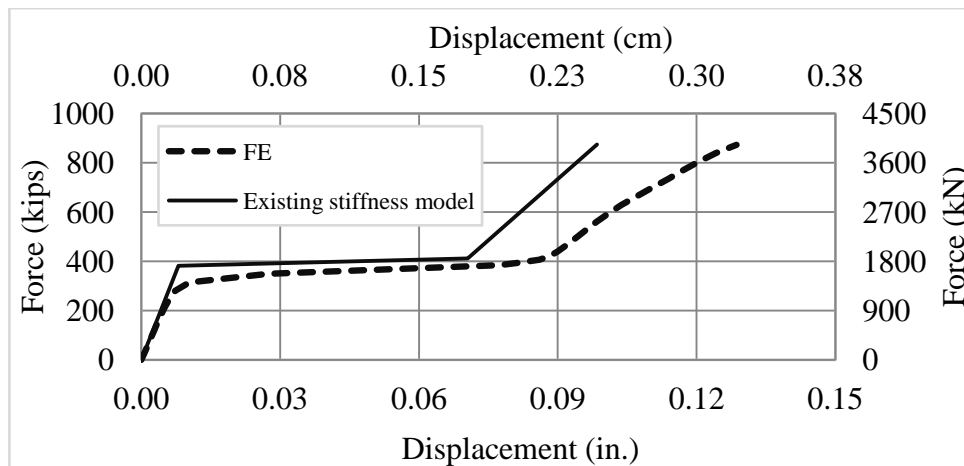
Fig. 9 – Existing slip and bearing stiffness model versus FE results for built-up T-stubs associated with W30x108 beams.

D. Column flange stiffness model

1. Excluding continuity plates effect

In moment resisting frames, thick-flange T-stub connections are needed with deep girders to resist the large moment expected. This may lead to a connection in which the T-stub flange is thicker than the column flange. In such cases, the column flange is subjected to bending, and may undergo significant deformations. This behavioral characteristic of the column flange causes the secondary prying phenomenon. A stiffness model for predicting the strength, stiffness, and ductility of column flange with and without continuity plates considering the effect of secondary prying is needed for seismic design. The following proposed stiffness model is based on the results obtained from the FE and experimental results.

a. Bolt stiffness

The bolt stiffness model proposed by Hantouche et al. [10] and Swanson and Leon [15] with some modification is used to incorporate the change in stiffness of the tension bolts throughout the loading history of the column flange. The model is composed of four linear segments. The first segment models the bolt in the pretension step, the second segment models the bolt in the elastic range, the third segment models the bolt after first yielding has been reached and the fourth segment models the bolt in the plastic range. The stiffness in the elastic is computed based on the assumption that the bolt can be simulated by an axial spring. The stiffnesses of the other segments were taken as ratios of the elastic stiffness based on a series of experiments data performed by Hantouche et al. (2012) [2].

The stiffness of the bolt in the pretension step was considered as 5 times the elastic

stiffness assuming that the bolt is rigid when subjected to compression. The following

relationships are used to describe the bolt stiffness:

Bolt Force (kip or kN) **Bolt Stiffness (kip/in. or kN/cm)**

$0 \le B \le B_0$ $\qquad\qquad\qquad K_{b,1} = 5K_b$ $\qquad\qquad\qquad\qquad$ (15)

$B_0 \le B \le 0.95B_n$ $\qquad\qquad K_{b,2} = K_b$ $\qquad\qquad\qquad\qquad$ (16)

$0.95B_n \le B \le B_n$ $\qquad\qquad K_{b,3} = 0.1K_b$ $\qquad\qquad\qquad\qquad$ (17)

$B_n \le B \le B_{fracture}$ $\qquad\qquad K_{b,4} = 0.03K_b$ $\qquad\qquad\qquad\qquad$ (18)

where B (kips or kN) is the current force in the tension bolt, B_0 (kips or kN) is the

minimum pretension force per bolt as specified by ANSI/AISC 360 [19], B_n (kips or kN) is

the tensile capacity of the bolt, $B_{fracture}$ (kips or kN) is the fracture load of the bolt, and K_b

(kips/in. or kN/cm) is the stiffness of the bolt in the elastic range.

b. Elastic-plastic column flange model

A model that uses geometrical and mechanical properties consistent with previous

stiffness models that are based on incremental analysis is presented. The model predicts

the response of the column flange as yielding starts and the plastic zone penetrates through

its thickness. Nonlinear material behavior and shear deformation are accounted for in the

formulation.

The column flange response is modeled analytically on the basis of a beam

representation for the flange, a multi-linear spring for the bolts, and accounting for the

contact phenomenon that occurs between the T-stub flange (assumed rigid) and the column

flange. The model considers the limit states of fully plastic hinges forming near the K-zone and at the bolt line. The secondary prying force at the tip of the flange was simulated using pin supports. Fig. 10 shows the column flange model proposed to characterize its force-deformation behavior.
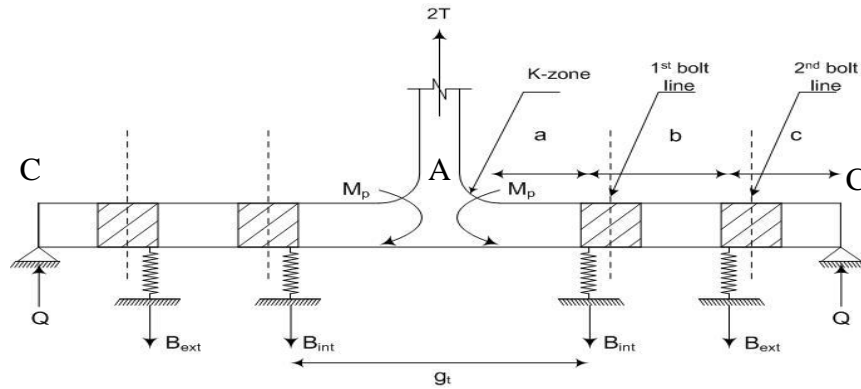
Fig. 10 – Complete column flange geometry.

The system is loaded by applying a vertical force at point A (K-zone). The change of the reaction load at point C (column flange tip) at every load increment is the prying gradient, and the reaction load at failure of the bolts is the secondary prying force. The ratio of the applied force, T, at point A (K-zone) to the displacement, $\varDelta$, of point A (K-zone) is the stiffness of the column flange. The location of the linear spring is assumed to occur at a distance of half bolt diameter $(d_b/2)$ away from the bolt centerline as shown in Fig. 10.

Several failure modes of the column flange are possible. Fig. 11 shows the decision tree of the possible column flange states considered in this research. Note that the subscripts used for the stiffness term in the decision tree correspond to the state of the

column flange at the K-zone and bolt line and to the state of the tension bolts. For example, $k_{eee,kk}$, represents the stiffness of the column flange when it is still in its elastic range with both tension bolts in the kth stiffness state. Whereas the term, $k_{pee,kk}$, represents the stiffness of the column flange when plastification has occurred at the K-zone and both tension bolts are in the kth stiffness state.
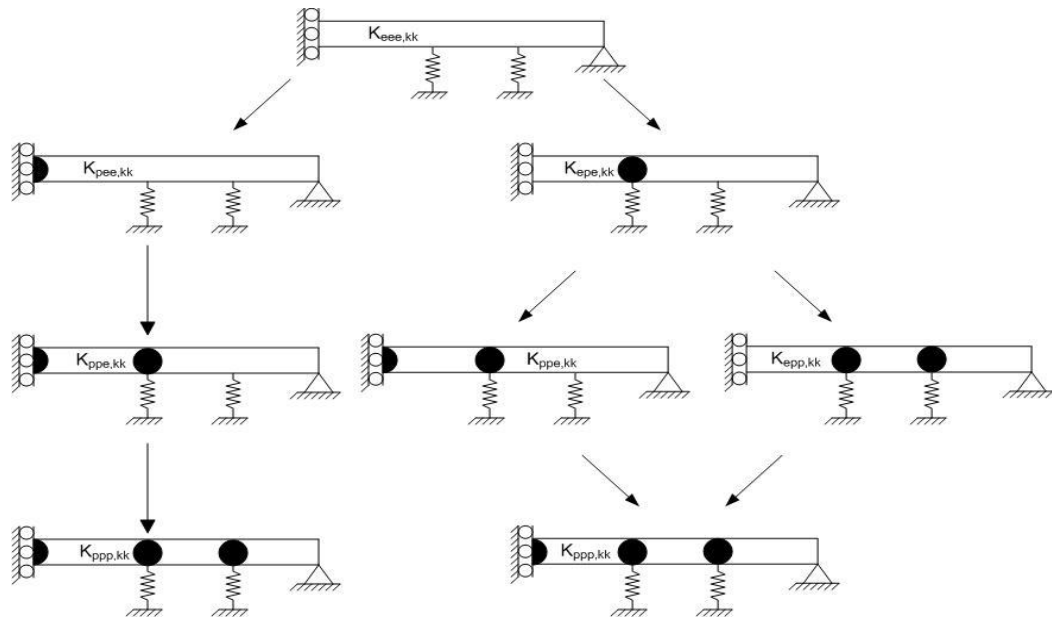
Fig. 11 – Decision tree for half column flange.

According to the detailed FE investigation performed by Hantouche et al. [2,8], full plastification of the column flange occurred only at the K-zone, and both the bolt lines were still in their elastic range when interior tension bolt fracture occurred for all the tested cases. Note that the stiffness terms corresponding to the state of full plastification of the bolt lines were not derived since they are not applicable for the cases studied in this research.

28

The following series of equations represent the stiffness, $K_{eee,kk}$, the change in the interior and the exterior bolt force ΔB_{int} and ΔB_{ext} respectively, the change in the moment at the K-zone, $\Delta M_{K\text{-}zone}$, and the prying gradient, ΔQ, terms for different column flange limit states:

i. Elastic column flange limit state

$$\Delta Q = \frac{\Delta T}{\left(\dfrac{a^3 \gamma_1}{6EI} - \dfrac{a(a+b+c)^2 \gamma_1}{2EI} + \dfrac{\gamma_1 \gamma_2 ac^2}{2EI\gamma_3} - \dfrac{f_s a \gamma_1}{GA} + \dfrac{\gamma_2}{\gamma_3} - 1 \right)} \tag{19}$$

$$\Delta B_{int} = \frac{\Delta Q \gamma_2}{\gamma_3} \tag{20}$$

$$\Delta B_{ext} = \left(\frac{\Delta Q a^3}{6EI} - \frac{\Delta Q a (a+b+c)^2}{2EI} + \frac{\Delta B_{int} ac^2}{2EI} - \frac{f_s \Delta Q a}{GA} \right) \gamma_1 \tag{21}$$

$$\Delta M_{K\text{-}zone} = \Delta T (b+c) - \Delta B_{int} b - \Delta Q a \tag{22}$$

$$K_{eee,kk} = \frac{1}{\gamma_7} \tag{23}$$

$$\gamma_1 = \frac{1}{\left(\dfrac{1}{K_{b1,k}} - \dfrac{a(b+c)^2}{2EI} \right)} \tag{24}$$

$$\gamma_2 = \frac{(a+b)^3}{6EI} - \frac{a^3 b^3 \gamma_1}{36(EI)^2} + \frac{ab^3(a+b+c)^2 \gamma_1}{12(EI)^2} + \frac{ab^3 f_s \gamma_1}{6EIGA} - \frac{(a+b)(a+b+c)^2}{2EI} + \frac{a^3(a+b)(b+c)^2 \gamma_1}{12(EI)^2} - \frac{a(a+b)(b+c)^2(a+b+c)^2 \gamma_1}{4(EI)^2} + \gamma_4 \tag{25}$$

$$\gamma_3 = \left(\frac{1}{K_{b2,k}} + \frac{ab^3 c^2 \gamma_1}{12(EI)^2} - \frac{(a+b)c^2}{2EI} - \frac{ac^2(a+b)(b+c)^2 \gamma_1}{4(EI)^2} - \frac{abc^2 f_s \gamma_1}{2GAEI} \right) \tag{26}$$

$$\gamma_4 = -\frac{a(a+b)(b+c)^2 f_s \gamma_1}{2GAEI} - \frac{(a+b)f_s}{GA} + \frac{a^3 b f_s \gamma_1}{6EIGA} - \frac{ab(a+b+c)^2 f_s \gamma_1}{2GAEI} - \left(\frac{f_s}{GA} \right)^2 ab\gamma_1 \tag{27}$$

$$\gamma_5 = \frac{a^3 \gamma_1}{6EI} - \frac{a(a+b+c)^2 \gamma_1}{2EI} + \frac{\gamma_1 \gamma_2 ac^2}{2EI\gamma_3} - \frac{f_s a \gamma_1}{GA} + \frac{\gamma_2}{\gamma_3} - 1 \tag{28}$$

$$\gamma_6 = \frac{a^3}{6EI\gamma_5} - \frac{a(a+b+c)^2}{2EI\gamma_5} + \frac{\gamma_2 ac^2}{2EI\gamma_3\gamma_5} - \frac{f_s a}{GA\gamma_5} \tag{29}$$

$$\gamma_7 = \left[\frac{(a+b+c)^3}{6\gamma_4} - \frac{\gamma_1\gamma_6(b+c)^3}{6} - \left(\frac{\gamma_2 c^3}{6\gamma_3\gamma_4} \right) + \gamma_8 \right] \left(\frac{1}{EI} \right) + \gamma_9 \tag{30}$$

$$\gamma_8 = \left(\frac{f_s}{GA} \right) \left(-\left(\frac{a+b+c}{\gamma_4} \right) + \gamma_1\gamma_6(b+c) + \left(\frac{\gamma_2 c}{\gamma_3\gamma_4} \right) \right) \tag{31}$$

$$\gamma_9 = \left(\left(\frac{-(a+b+c)^2}{2\gamma_4} \right) + \frac{\gamma_1\gamma_6(b+c)^2}{2} + \left(\frac{c^2\gamma_2}{2\gamma_3\gamma_4} \right) \right)(a+b+c) \tag{32}$$

ii. Plastic hinge formation at K-zone of the column flange limit state

$$\Delta Q = \Delta T \left(1 - \frac{b+c}{bK_{b2,k}\gamma_{10}} - \frac{b+c}{b} \right) \left(\frac{1}{\gamma_{11}} \right) \tag{33}$$

$$\Delta B_{int} = \frac{\Delta T(b+c)}{b} - \frac{\Delta Qa}{b} \tag{34}$$

$$\Delta B_{ext} = \left(\frac{\Delta B_{int}}{K_{b2,k}} - \frac{\Delta Q(a+b)^3}{6EI} - \frac{\Delta Q f_s(a+b)}{GA} + \frac{\Delta Q a^2(a+b)}{6EI} + \frac{\Delta Q f_s(a+b)}{GA} \right) \left(\frac{1}{\gamma_{10}} \right) \tag{35}$$

$$K_{pee,kk} = \frac{1}{\gamma_{14}} \tag{36}$$

$$\gamma_{10} = \left(\frac{a+b}{aK_{b1,k}} - \frac{b^3}{6EI} + \frac{f_s b}{GA} \right) \tag{37}$$

$$\gamma_{11} = \left(\frac{-a}{bK_{b2,k}\gamma_{10}} - \frac{(a+b)^3}{6EI\gamma_{10}} + \frac{a^2(a+b)}{6EI\gamma_{10}} - 2 \right) \tag{38}$$

$$\gamma_{12} = \left(1 - \frac{b+c}{bK_{b,2k}\gamma_{10}} - \frac{b+c}{b} \right) \left(\frac{1}{\gamma_{11}} \right) \tag{39}$$

$$\gamma_{13} = \frac{\frac{b+c-a\gamma_{12}}{b}}{K_{b,2k}} - \frac{(a+b)^3\gamma_{12}}{6EI} - \frac{f_s(a+b)\gamma_{12}}{GA} + \frac{a^2(a+b)\gamma_{12}}{6EI} + \frac{f_s(a+b)\gamma_{12}}{GA} \tag{40}$$

$$\gamma_{14} = \frac{(a+b+c)^3\gamma_{12}}{6EI} - \frac{(b+c)^3\gamma_{13}}{6EI\gamma_{10}} - \left(\frac{c^3}{6EI} \right) \left(\frac{b+c-a\gamma_{12}}{b} \right) + \gamma_{15} + \gamma_{16} \tag{41}$$

$$\gamma_{15} = \left(\frac{f_s}{GA} \right) \left((a+b+c)\gamma_{12} + (b+c) \left(\frac{\gamma_{13}}{\gamma_{10}} \right) + \left(\frac{b+c-a\gamma_{12}}{b} \right) c \right) \tag{42}$$

$$\gamma_{16} = \left(\left(\left(\frac{1}{K_{b1,k}a} \right) \left(\frac{\gamma_{13}}{\gamma_{10}} \right) - \frac{a^2\gamma_{12}}{6EI} + \frac{f_s\gamma_{12}}{GA} \right) \left(a + b + c \right) \right) \tag{43}$$

where $\varDelta T$ (kips or kN) is the change in the applied load, a (in. or cm) is the length

of a column flange measured from the inside edge of the exterior bolt line to the outside

edge of the column flange, b (in. or cm) is the gage distance between the tension bolts, c

(in. or cm) is the length of the column flange measured from the inside edge of the interior

bolt to the location of occurrence of the plastic hinge at the K-zone of the column flange,

$\gamma_1, \gamma_2, \gamma_3, \gamma_4, \gamma_5, \gamma_6, \gamma_7, \gamma_8, \gamma_9, \gamma_{10}, \gamma_{11}, \gamma_{12}, \gamma_{13}, \gamma_{14}, \gamma_{15}$ and γ_{16} are constants used in the

calculation of the column flange stiffness, A (in^2 or cm^2) is the cross sectional area, f_s is the

shape factor used in computing the shear deformations, G (ksi or MPa) is the shear

modulus of elasticity, I (in^4 or cm^4) is the second moment of inertia of a cross section, $K_{b1,k}$

(kips/in. or kN/cm) represents the stiffness of the interior bolt in the kth range, and $K_{b2,k}$

(kips/in. or kN/cm) represents the stiffness of the exterior bolt in the kth range. Note that

from the FE investigation performed by Hantouche et al. [2, 8], it was determined that the

plastic hinge forms at a distance of ¼ in. away from the middle of the column web.

The stiffness terms were derived to be applied in an incremental computer

automated iterative solution as shown in Fig. 12. At the beginning of the loading step, the

flange is still in its elastic state. An engineer would start by determining the elastic

stiffness of the flange $k_{eee,kk}$. Next, several checks need to be made to determine which

limit state will be reached first. The possible limit states are: (1) full plastification of the

K-zone, (2) yielding of the interior bolt, (3) yielding of the exterior bolt, and (4) separation

of the column flange and T-stub flange. Then, the prying gradient, the moment at the K-

zone and the forces in the interior and exterior bolts corresponding to the current load step are computed. Finally, incremental displacement corresponding to the current load step is calculated, and the new stiffness is determined and the process is repeated again until the bolt force reaches $B_{fracture}$. The entire procedure is illustrated in Fig. 12.

Calculate the Elastic Stiffness K_{ee}
Begin Load Step

Check Possible Limit States

Plastification at K-zone

1st Yielding of the Interior Bolt

Assume Load Step $\Delta T1$

Assume Load Step $\Delta T2$

Adjust Load Step $\Delta T1$

Calculate ΔQ Using Eq (10)

Calculate ΔB_{int} Using Eq (11)

Calculate ΔB_{ext} Using Eq (12)

Calculate ΔM_{K-zone} Using Eq (13)

Does $M_{K-zone} = M_p$?

No

Calculate ΔQ Using Eq (10)

Calculate ΔB_{int} Using Eq (11)

Does $B_{int} = 0.95 B_n$?

No

Adjust Load Step $\Delta T2$

Is $\Delta T1 < \Delta T2$?

Yes

Yes

Yes

No

Load Step = $\Delta T1$

Calculate ΔQ Using Eq (24)

Calculate ΔB_{int} Using Eq (25)

Calculate ΔB_{ext} Using Eq (26)

Load Step Finished

Load Step = $\Delta T2$

Calculate ΔQ Using Eq (10)

Calculate ΔB_{int} Using Eq (11)

Calculate ΔB_{ext} Using Eq (12)

Calculate ΔM_{K-zone} Using Eq (13)

Load Step Finished

Adjust bolt stiffness

Assume Load Step $\Delta T3$

Check Yielding of Interior Bolt

No

Assume Load Step $\Delta T4$

Check Yielding of Exterior Bolt

No

Yes

Is $\Delta T3 < \Delta T4$?

Yes

Yes

No

Load Step = $\Delta T3$

Calculate ΔQ, ΔB_{int}, and ΔB_{ext},

Load Step Finished

Repeat Process Until $B_{int} = B_{fracture}$

Load Step = $\Delta T4$

Calculate ΔQ, ΔB_{int}, and ΔB_{ext},

Load Step Finished

Repeat Process Until $B_{int} = B_{fracture}$

Assume Load Step $\Delta T3$

Check Yielding of Interior Bolt

No

Assume Load Step $\Delta T4$

Check Yielding of Exterior Bolt

No

Yes

Is $\Delta T3 < \Delta T4$?

Yes

Yes

No

Load Step = $\Delta T3$

Calculate ΔQ, ΔB_{int}, and ΔB_{ext},

Load Step Finished

Repeat Process Until $B_{int} = B_{fracture}$

Load Step = $\Delta T4$

Calculate ΔQ, ΔB_{int}, and ΔB_{ext},

Load Step Finished

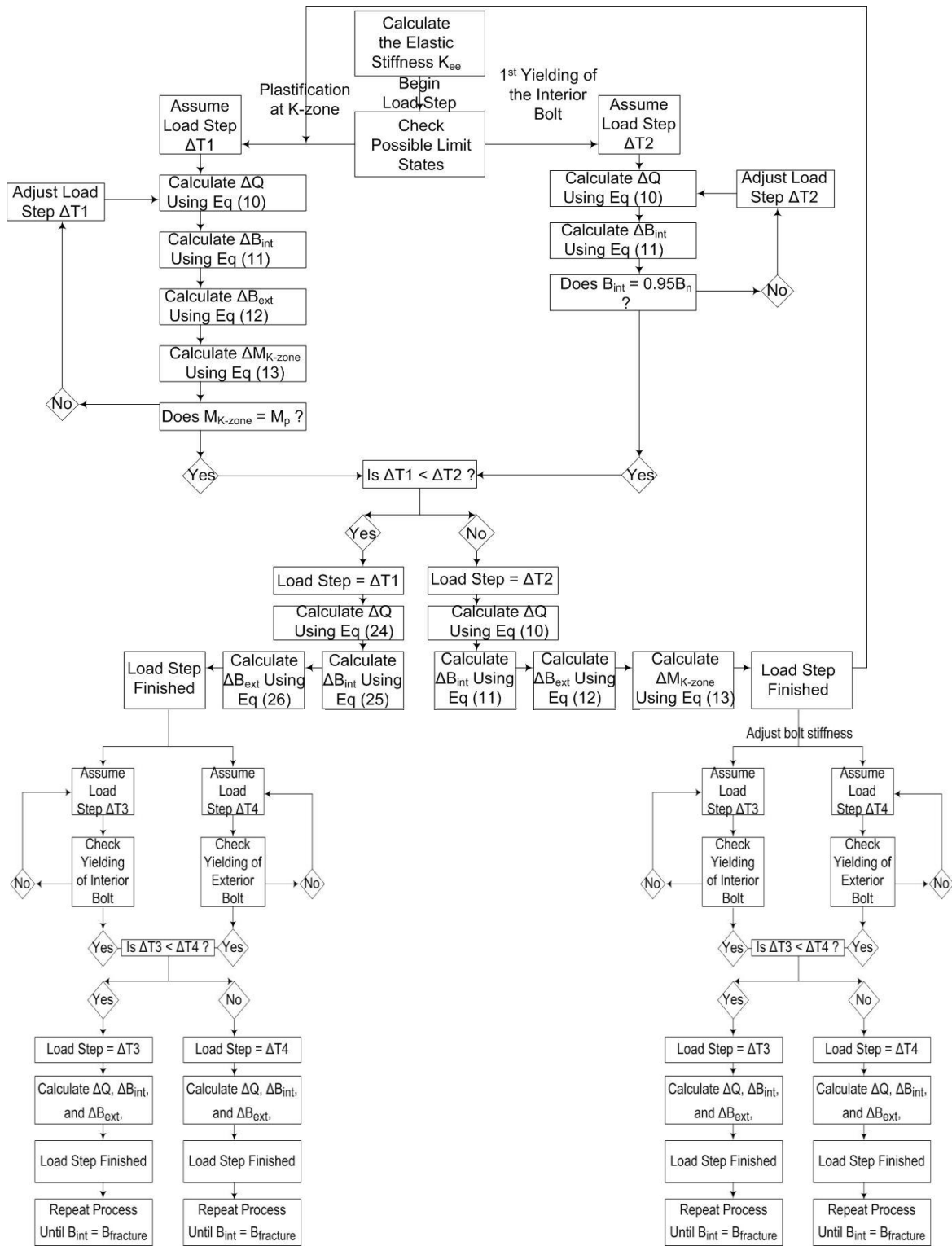Repeat Process Until $B_{int} = B_{fracture}$

Fig. 12 – Flowchart of the incremental stiffness column flange model.

After determining the amount of secondary prying using the stiffness model

above, the tension bolt diameter is recomputed to account for the additional force

introduced to the bolts due to secondary prying effect. This is done by increasing the

applied load by the amount of secondary prying and thus the new bolt diameter can be

computed. Note that limit states (3) and (4) were not included in the analysis since the FE

results shows that those limit states are not possible for the cases studied.

c. Model performance

The performance of the column flange model was assessed by comparing the

model predictions with the FE analysis results generated by Hantouche et al. [8] for thick

built-up T-stubs associated with deep girders. The FE results were validated against

experimental results performed by Hantouche et al. [2] and are deemed valid for

comparison with the stiffness model results. Note that the cases considered in this analysis

cover all the range of deep girders according to the current design practice.

Figs. 13(a) and 13(b) show a comparison of the proposed stiffness model versus

the FE results for thick built-up T-stubs associated with W24x76 and W30x108 beams,

respectively. The proposed stiffness model predicts interior tension bolt fracture after full

plastification of the column flange K-zone for both W24x76 and W30x108 beams at an

applied load of 755 kips (3358 kN) and 787 kips (3500 kN), respectively. This is around

1% and 6% less than the failure load predicted by the FE which are 765 kips (3403 kN)

and 838 kips (3727 kN), respectively. The ultimate deformation predicted by the proposed

model is 0.15 in. (0.36 cm) and 0.14 in. (0.35 cm) for W24x76 and W30x108 beams,

respectively. This is around 11% and 14% less than the ultimate deformation predicted by

the FE models which are 0.16 in. (0.41 cm) and 0.15 in. (0.38 cm), respectively. This

difference can be due to the fact that the column flange was modeled as a beam in the

proposed column flange stiffness model which results in additional bending in the bolts

predicted by the column flange model, and thus predicts the failure of the tension bolts at a

lower load, and therefore resulting in a stiffer behavior. Furthermore, when applying the

proposed column flange stiffness model the parameter, p, corresponding to the tributary

area per bolt, was assumed to be equal to half of the breadth of the T-flange which does not

reflect the complexity of the stress distribution in the column flange which propagates

through the height of the column flange as the load increases.

(a)
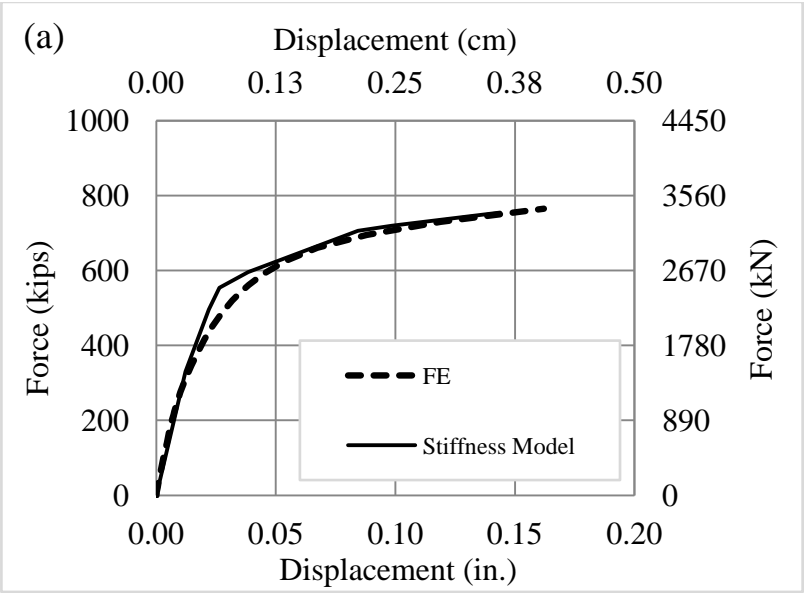
Fig. 13 – Comparison of the FE results with the proposed column flange stiffness model: (a) associated with W24x76 beam with $t_{cf}/t_{Tf} = 0.60$, (b) associated with W30x108 beam with $t_{cf}/t_{Tf} = 0.67$

The proposed stiffness model predicts full plastification of the column flange K-zone followed by yielding of the interior tension bolts. Loading continues until yielding of the exterior bolts occurs. Finally, at a certain load level the interior tension bolts fracture.

Fig. 14 shows a comparison of the results obtained by the column flange model and the FE analysis for a W24x76 girder having a ratio of column flange thickness to T-stub flange thickness t_{cf}/t_{Tf} equal to 0.90. The proposed model predicts failure of the interior tension bolts at an applied load of 658 kips (2927 kN) which conforms to the FE results. This is around 5% less than the failure load predicted by the FE analysis which is 698 kips (3103 kN). In addition, the model predicts a deformation at failure of 0.06 in. (0.15 cm). It can be clearly seen that the deformation predicted by the column flange model is negligible compared to the deformation that occurs in the column flange for the

36

case where t_{cf}/t_{Tf} is less than 1 which conforms to the study performed by Hantouche et al. [8].
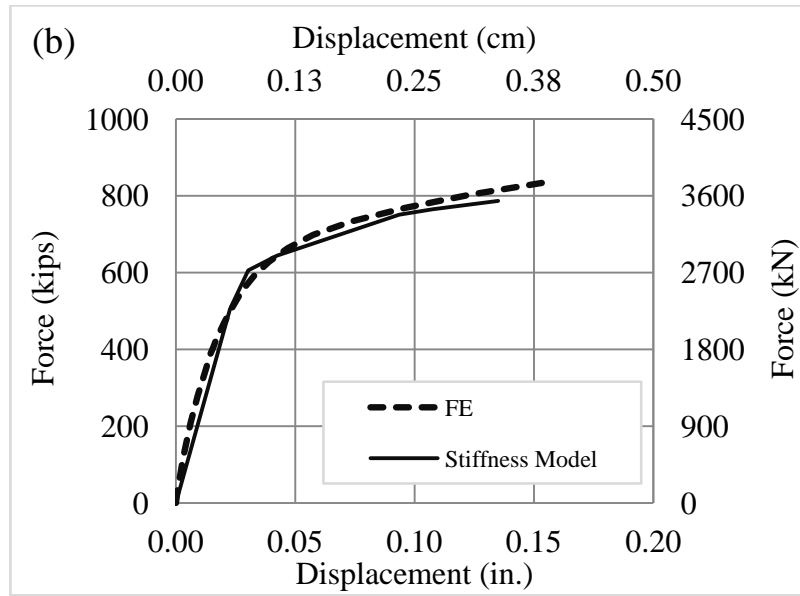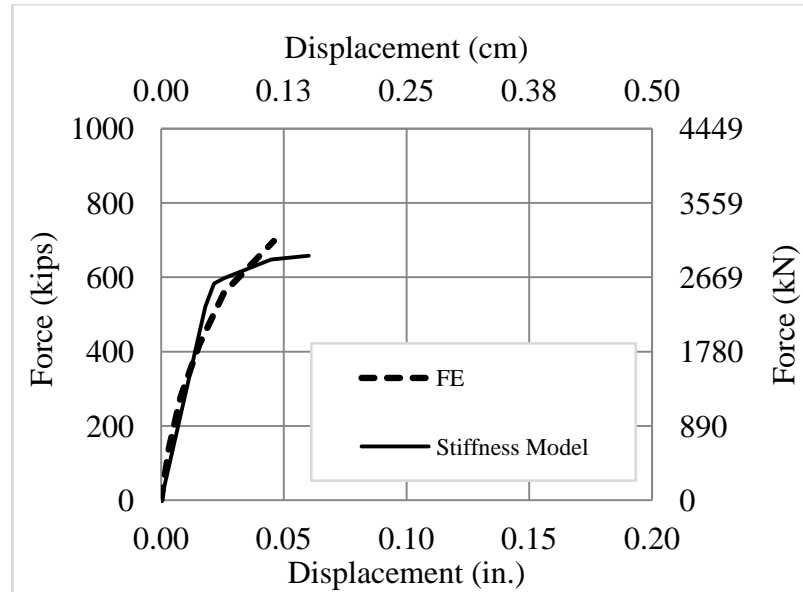

Fig. 14 – Comparison of the FE results with the proposed column flange stiffness model associated with W24x76 beam with $t_{cf}/t_{Tf} = 0.90$.

2. Including continuity plates effect

Continuity plates are usually provided in steel connections to stiffen the column flange and web which results in a reduction in the overall ductility of the connection. Several experimental programs [5, 24-26] have been conducted on bolted T-stub connections including continuity plates to study the behavior of the system under monotonic and cyclic loading. The results of these studies show no significant deformation from the column flange side. In addition, according to the detailed FE investigation performed by Hantouche et al. [8] on bolted thick built-up T-stub connections, it was shown that for the cases where continuity plates are provided, the

37

deformation from the column flange is negligible and therefore secondary prying effect is not significant. The cases investigated in the study above included deep beams with depth ranging from 24 in. (60 cm) till 36 in. (90 cm), having t_{cf}/t_{Tf} ranging from 0.60 to 1.33. In order to account for the additional stiffness in the column flange due to the continuity plates, a relationship was developed to relate the elastic stiffness of the force-deformation curve of the column flange with and without continuity plates as a function of t_{cf}/t_{Tf}. The study included 4 cases with t_{cf}/t_{Tf} ranging between 0.60 and 1.20. The following relationship has been obtained with an $R^2=0.94$:

$$K_{cp,eee} = K_{eee,kk}\left(1.5\left(\frac{t_{cf}}{t_{Tf}}\right) + 0.7 \right) \tag{44}$$

where $K_{cp,eee}$ (kips/in or kN/cm) is the elastic stiffness of the column flange including continuity plates, t_{cf} (in. or cm) is the thickness of the column flange, and t_{Tf} (in. or cm) is the thickness of the T-stub flange.

E. Total assembly

After each of the different deformation mechanisms has been computed, the total force-deformation curve of the connection is obtained by assembling the contribution from individual components at common incremental loads. Linear interpolation is used to make sure that all load points from all the component stiffness models are included in the total force-deformation curve. Fig. 15 shows a comparison of the total force-deformation curve obtained from the stiffness model and the FE analysis results for thick built-up T-stubs associated with W24x76 girders with a ratio t_{cf}/t_{Tf} equal to 0.67.
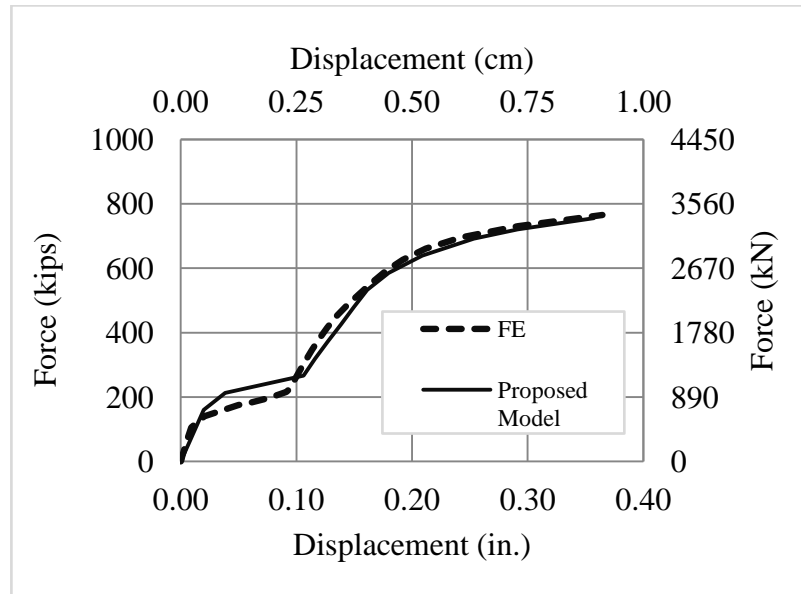
Fig. 15 – Total connection deformation associated with W24x76 beam including column flange deformation.

The proposed stiffness model predicts the force-deformation response of the T-stub/column flange system with excellent agreement when compared with FE results. In addition, the model predicts an ultimate capacity of the connection of 755 kips (3358 kN) which is around 1% lower than the actual capacity predicted by the FE analysis which is 765 kips (3403 kN). The model also predicts an ultimate deformation of 0.36 in. (0.91 cm) which is around 2% lower than the actual deformation predicted by the FE analysis which is 0.37 in. (0.94 cm).

F. Model limitations

The proposed stiffness model is based on rational mechanistic assumptions and experimental and FE results. Simplifications and assumptions were made to reduce the complexity level of the problem. Therefore, some limitations exist:

- The proposed T-stem model only applies to thick built-up T-stubs associated with deep girders ranging from W24 to W36 depth.

- The column flange model is very sensitive to the material properties of the tension bolts, thus accurate knowledge of the material properties being used is preferable when using the proposed column flange model to predict the force-deformation curve.

- When using the column flange model, the tributary area per tension bolt was assumed to be located around the tension bolt holes due to stress concentrations around the holes. Although this assumption does not reflect the true complexity of the stress distribution in the column flange, however, acceptable results were achieved.

CHAPTER IV

COLUMN FLANGE STRENGTH MODEL

The possible failure modes of the column flange are: (1) formation of a plastic

hinge at the K-zone followed by fracture of the interior tension bolts, (2) formation of a

plastic hinge at the 1st bolt line followed by fracture of the interior tension bolts, (3) full

plastification of the column flange, and (4) pure tension bolt fracture. The FE analysis

performed by Hantouche et al. [8] thick built-up T-stub connections showed that when the

ratio t_{cf}/t_{Tf} ranges between 0.6 and 1, failure mode (1) occurs. A strength model that

predicts the capacity of the column flange including secondary prying effect when failure

mode (1) occurs is developed. Fig. 10 shows the state of the column flange at failure when

failure mode (1) occurs. Moment equilibrium of the column flange results in the

expression below:

$$T\left(a+b+c\right) = B_{1n}c + B_{2n}\left(b+c\right) + M_{K-zone} \tag{45}$$

where B_{1n} (kips or kN) is the tensile capacity of the exterior tension bolt, and B_{2n}

(kips or kN) is the tensile capacity of the interior tension bolt.

At failure of the interior bolts, the moment at the K-zone, M_{K-zone}, is equal to the

plastic moment capacity of the column flange, M_p, and can be written as follows:

$$M_p = \left(\frac{t_{cf}\, p^2}{4}\right) F_y \tag{46}$$

Equations (45) and (46) yield the ultimate capacity of the column flange.

$$T = \frac{B_{1n}c}{a+b+c} + \frac{B_{2n}(b+c)}{a+b+c} + \frac{F_y t_{cf} p^2}{4(a+b+c)} \tag{47}$$

The performance of the column flange strength model was validated by comparing the model predictions with the FE analysis results performed by Hantouche et al. [8] for thick built-up T-stubs associated with W24x76 and W30x108 girders having a ratio, t_{cf}/t_{Tf}, of 0.60 and 0.67, respectively. The proposed strength model predicts an ultimate capacity of the column flange for W24x76 and W30x108 beams of 752.60 kips (3348 kN) and 967 kips (4301 kN), respectively. This is around 2% less and 13% higher than the ultimate capacity predicted by the FE model. Note that the proposed strength model will be further validated in the future against experimental results.

CHAPTER V

ENERGY DISSIPATION

A. Energy dissipation T-stub/column flange system: A closed-form model

1. Energy dissipation from the T-stub

Energy dissipation is defined as the area under the outer hysteresis loop in a cyclic test. The prediction of the energy dissipation of a connection is important as it enables the designers to predict the overall connection ductility and thus leads to an appropriate design where the rotation demand is adequate with the rotation capacity [3]. Many research studies have been conducted on bolted T-stub connections under cyclic loading aiming at identifying the geometric and mechanical parameters affecting the behavior of T-stub connections under cyclic loading [12,20-21, 27]. In addition, Piluso and Rizzano [3] proposed a model to predict the force-deformation curve of the T-stub connection under cyclic loading knowing its geometrical and mechanical properties. The model predicts the behavior of the connection under cyclic loading once rules for strength and stiffness degradation are established and the monotonic behavior of the connection have been derived. According to the experimental results obtained by Hantouche et al. [2], thick built-up T-stub connections have similar behavior under monotonic and cyclic loading. This was validated by computing the values for the stiffness degradation, which is defined as the change in the initial stiffness of the force-deformation curve under cyclic loading between the first and the last cycle, the failure modes for different specimens under monotonic and cyclic loading and the ultimate capacity of the connection under monotonic

and cyclic loading. Table 1 summarizes these values. Note that for some of the cases

considered in this research, the values for the stiffness degradation could not be calculated,

because of some noise in the cyclic data, and thus were not reported.

Table 1 -Comparison of the monotonic and cyclic results

Specimen	Stiffness Degradation after the Last Cycle	Ultimate Capacity Under Monotonic Load	Failure Mode Under Monotonic Load	Ultimate Capacity Under Monotonic Load	Failure Mode Under Monotonic Load
TMCS-01/ TCCS-01	3.6 %	280.7 kips (1250 kN)	Net Section Fracture	281.4 kips (1252 kN)	Net Section Fracture
TMCS-02/ TCCS-02	17.0 %	281.8 kips 1254 (kN)	Net Section Fracture	285.5 kips (1270 kN)	Net Section Fracture
TMFS-01/ TCFS-01	7.0 %	282.6 kips (1258 kN)	Net Section Fracture	280.0 kips (1246 kN)	Net Section Fracture
TMFS-02/ TCFS-02	8.9 %	277.9 kips (1237 kN)	Net Section Fracture	280.1 kips (1247 kN)	Net Section Fracture
TMFS-03/ TCFS-03	10.3 %	263.3 kips (1172 kN)	Net Section Fracture	271.0 kips (1206 kN)	Net Section Fracture
TMFS-04/ TCFS-04	3.9 %	264.2 kips (1176 kN)	Net Section Fracture	267.6 kips (1191 kN)	Net Section Fracture
TMFL-03/ TCFL-03	9.4 %	394.6 kips (1756 kN)	Tension Bolt Fracture	-	Tension Bolt Fracture

It can be seen that for most studied cases the failure mode is identical under

monotonic and cyclic tests. In addition, the ultimate capacity of the connection is identical

under monotonic and cyclic load. From the results, it can be seen that the stiffness after

the last cycle is almost equal to the initial stiffness, and therefore the stiffness degradation

for the case of thick built-up T-stub connections can be neglected as shown in Figs. 16(a)

and 16(b). Finally, based on the experimental results performed by Hantouche et al [2], no

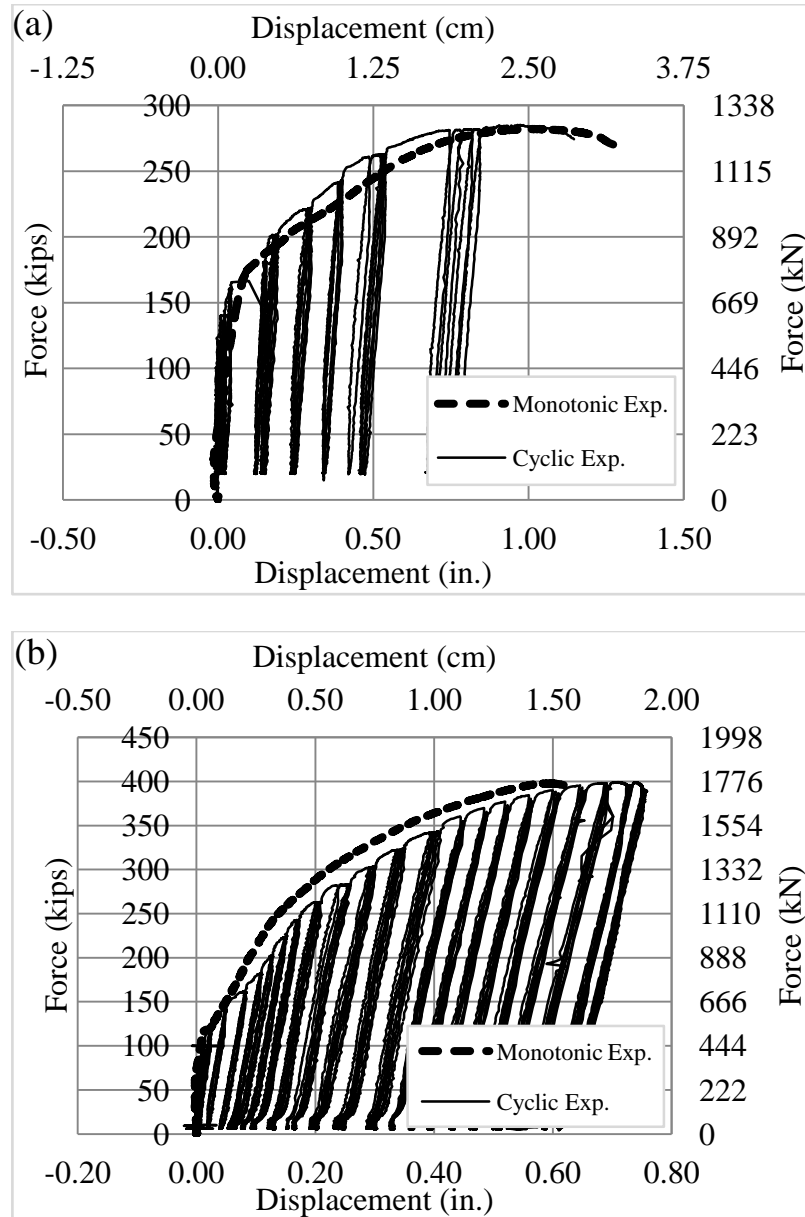sudden slip was observed under cyclic loading.

Fig. 16 – Comparison of the monotonic and cyclic load/deformation curve for thick built-up T-stub connections: (a) with T-stem thickness of 3/4 in. (TMCS-02/TCCS-02) [22-23], (b) with T-stem thickness of 1-1/4 in. (TMFL-03/TCFL-03) [22-23].

From the FE investigation and experimental results performed by Hantouche et al. [2,8], two failure modes were associated with thick built-up T-stub connections associated with deep girders: (1) T-stem fracture, and (2) tension bolt fracture. Based on these failure modes, eight scenarios were identified depending on: (1) the limit state of the T-flange and T-stem at failure of the connection, and (2) the occurrence of the relative slip between the beam flange and the T-stem. The following equations are used to predict the T-stub energy dissipation capacity, E_D, depending on the governing yielding mechanisms and the failure modes of the connection:

Case 1

$$E_D = \frac{1}{2} \frac{P_u^2}{K_{e,stem}} + \frac{1}{2} \frac{P_{y,flange}^2}{K_{e,flange}} + \lambda_1 \tag{48}$$

Case 2

$$E_D = \frac{1}{2} \frac{P_u^2}{K_{e,stem}} + \frac{1}{2} \frac{P_{y,flange}^2}{K_{e,flange}} + \lambda_1 + \lambda_2 \tag{49}$$

Case 3

$$E_D = \frac{1}{2} \frac{P_{y,stem}^2}{K_{e,stem}} + \frac{1}{2K_{p,stem}}\left(P_u^2 - P_{y,stem}^2\right) + \frac{1}{2} \frac{P_{y,flange}^2}{K_{e,flange}} + \lambda_1 \tag{50}$$

Case 4

$$E_D = \frac{1}{2} \frac{P_{y,stem}^2}{K_{e,stem}} + \frac{1}{2K_{p,stem}}\left(P_u^2 - P_{y,stem}^2\right) + \frac{1}{2} \frac{P_{y,flange}^2}{K_{e,flange}} + \lambda_1 + \lambda_2 \tag{51}$$

Case 5

$$E_D = \frac{1}{2} K_{e,stem} P_{y,stem} + \frac{1}{2K_{p,stem}}\left(P_u^2 - P_{y,stem}^2\right) + \frac{1}{2} K_{e,flange} P_u \tag{52}$$

46

Case 6

$$E_D = \frac{1}{2}K_{e,stem}P_{y,stem} + \frac{1}{2K_{p,stem}}\left(P_u^2 - P_{y,stem}^2\right) + \frac{1}{2}K_{e,flange}P_u + \lambda_2 \tag{53}$$

Case 7

$$E_D = \frac{1}{2}\frac{P_{y,stem}^2}{K_{e,stem}} + \frac{1}{2K_{p,stem}}\left(P_u^2 - P_{y,stem}^2\right) + \frac{1}{2}\frac{P_{y,flange}^2}{K_{e,flange}} + \lambda_3 \tag{54}$$

Case 8

$$E_D = \frac{1}{2}\frac{P_{y,stem}^2}{K_{e,stem}} + \frac{1}{2K_{p,stem}}\left(P_u^2 - P_{y,stem}^2\right) + \frac{1}{2}\frac{P_{y,flange}^2}{K_{e,flange}} + \lambda_2 + \lambda_3 \tag{55}$$

$$\lambda_1 = \left(\frac{1}{L}\right)\left(F_y\frac{t_{Tf}^2}{4}\right)(\theta_u - \theta_y)(L) + \frac{F_y\varepsilon_y^2 t_{Tf}^2}{\theta_u L} - \frac{F_y\varepsilon_y^2 t_{Tf}^2}{3\theta_u L} \tag{56}$$

$$\lambda_2 = \frac{1}{2}\left[P_{slip} + \left(P_{slip} + 0.04K_{e,stem}P_{slip}\right)\right]\Delta_{slip} + \frac{1}{2K_{bearing}}\left[P_u^2 - \left(P_{slip} + 0.04K_{e,stem}P_{slip}\right)^2\right] \tag{57}$$

$$\lambda_3 = \left(\frac{1}{L}\right)\left(F_y\frac{t_{Tf}^2}{4}\right)(\theta_c - \theta_y)(L) + \frac{F_y\varepsilon_y^2 t_{Tf}^2}{\theta_c L} - \frac{F_y\varepsilon_y^2 t_{Tf}^2}{3\theta_c L} \tag{58}$$

where P_u (kips or kN) is the ultimate load of the T-stub, $P_{y,flange}$ (kips or kN) is the yield load of the T-flange, t_{Tf} (in. or cm) is the thickness of the T-flange, θ_u (rad/in. or rad/cm) is the rotation of the flange at which bolt fracture occurs, θ_c (rad/in. or rad/cm) is the rotation of the flange at which stem fracture occurs, θ_y (rad/in. or rad/cm) rotation of the flange at which partial yielding of the T-flange occurs, ε_y is the strain at yielding of the steel, P_{slip} (kips or kN) is the load that causes relative slip between the beam flange and the T-stem, Δ_{slip} (in. or cm) is the relative slip between the beam flange and the T-stem which

is equal to the hole clearance, L (in. or cm) is the moment arm for the T-flange, stiffness model, $K_{e,flange}$ (kips/in. or kN/cm) is the initial stiffness of the T-flange stiffness model, $K_{bearing}$ (kips/in. or kN/cm) is the bearing stiffness of the slip and bearing stiffness model, and λ_1, λ_2, and λ_3 are constants used for the calculation of the energy dissipation capacity of the T-stub.

The prediction of the energy dissipation capacity, E_D, of thick built-up T-stub connections associated with deep girders requires the following steps:

(1)   Prediction of the T-stem force-deformation curve using the proposed stiffness model in section 2.1;

(2)   Prediction of the T-flange force-deformation curve using the flange partial yielding stiffness model developed by Hantouche et al. [10];

(3)   Prediction of the slip and bearing force-deformation curve using Hu et al. [11] stiffness model;

(4)   Assembly of the monotonic force-deformation curve using the above component stiffness models;

(5)   Identifying the T-stem and T-flange state at failure of the connection;

(6)   Computation of the energy dissipation capacity of the T-stub using the Eqs. (48) to (58);

The performance of the energy dissipation model was validated by comparing the model predictions with the energy dissipation capacity values predicted from the experimental results [2] having T-stem thickness of ¾ in. (1.90 cm) and 1-1/4 in. (3.13 cm). The model accurately predicts the energy dissipation capacity of the thick built-up T-

stubs. The model predicts a value of 67 kips-in. (746 kN-cm) for thick built-up T-stubs

with T-stem thickness of 1-1/4 in. (3.13 cm) which is around 12% lower than the value

obtained from the experimental results which is 77 kips-in. (854 kN-cm). The model also

predicts an energy dissipation capacity of 146 kips-in. (1622 kN-cm) for thick-built-up T-

stubs with T-stem thickness of ¾ in. (1.90 cm) that is around 1% higher than the value

obtained from experimental results which is 145 kips-in. (1611 kN-cm).

2. *Energy dissipation from the column flange side without continuity plates*

After identifying the major parameters that impact the energy dissipation which

was found to be t_{cf}/t_{Tf}, cases were selected and modeled using ABAQUS. For cases where

t_{cf}/t_{Tf} is larger than 0.76 or when continuity plates are supplied, the contribution of the

column flange side to the total energy dissipation of the T-stub/column flange system is

considered negligible [8].

The results obtained showed that for cases where t_{cf}/t_{Tf} ranges between 0.60 to

0.76, the energy dissipation capacity from the column flange without continuity plates

ranges between 66% and 54% of the total energy dissipated, respectively. The results

showed that the column flange side has a significant contribution to the overall energy

dissipation capacity of the connection.

CHAPTER VI

CONCLUSIONS

From the FE and experimental results, as well as the models developed in this research, several conclusions can be draw:

- In designing thick flange T-stub connections associated with deep girders, all yielding mechanisms and failure modes are needed to be identified including secondary prying phenomenon which is considered a potential failure mode in connections studied in this research.

- A proposed stiffness model that predicts the force-deformation curve of thick T-stub/column flange system with and without continuity plates including secondary prying effect is developed.

- Also, a proposed strength model that predicts the capacity of the column flange for the failure mode of full plastification at the K-zone followed by interior bolt fracture is developed. The proposed stiffness and strength models show excellent agreement when comparing with experimental and FE results.

- Closed form expressions that predict the energy dissipation capacity of the connection with and without continuity plates were developed and showed excellent agreement when comparing with experimental results. The results show that the column flange contributes significantly to the overall ductility of the connection.

- This research provides engineers guidelines to design for the additional load induced in the tension bolts and for the maximum rotational capacity demand of the connection which are required in seismic analysis and design.

- This research also provides guidelines to detail connections without continuity plates (if other requirements were satisfied) which result in gaining additional ductility while satisfying the strength requirements.

- One of the main advantages of the proposed stiffness model is that, in addition to its accuracy, it requires much less computational effort than that required using FE analysis, and can be used as well in more advanced modeling applications for seismic analysis and design. The proposed column flange stiffness model can be easily implemented using any simple computer programming language.

Several areas o interest that are complimentary to this research work and that has not been investigated in this research can be done in the future. Thus, the following recommendations are suggested:

- Conduct an experimental program on thick built-up T-stubs including column flange deformation to further validate the proposed column flange model in this research.

- Use the results of the experimental program suggested above, along with the existing FE results, to develop strength models for the column for all possible failure modes.

- Develop stiffness models to characterize the behavior of the panel shear zone and the beam and include them in the overall behavior of the T-stub connection.

- Develop a complete cyclic stiffness model to characterize the unloading and reloading branches of the T-stub/column system behavior.

APPENDIX

I. SOURCE CODE

```
function [  ] = CF(
Ke1,Ke2,Ke3,Ke4,Ke5,Ke6,Ke7,Fy,p,tf,Bn,Bfract,B0,E,I,K1,K2,a,b,c,fs,G,A )
%CF Summary of this function goes here
%   Detailed explanation goes here

%Bint: Current Force in the Interior Bolt
%Bfract: Fracture Force of the Bolt
%DeltaT: Incremental Applied Load
%Q: Prying Force (Interior and Exterior Bolt)
%Bext: Current Force in the Exterior Bolt
%fs: Shape Factor for Shear Deformation
%G: Shear Modulus of Elasticity
%Mkzone: Current Moment at the K-zone
%Kiii: Corresponds to the Stiffness of the System with Respect to the State
%of the Bolt and the k-zone
%Mpbline: Plastic Moment at the Bolt Line
%Mpkzone: Plastic Moment at the Kzone
%Bn: Nominal Tensile Strength of the Bolt
%Mks: State of the K-zone
%B1s: State of the Interior Bolt
%B2s: State of the Exterior Bolt

%Define the Different Stiffness States for each Bolt
k1 = [0.1*K1 0.01*K1 0.01*K1];
k2 = [0.1*K2 0.01*K2 0.01*K2];

%Calculate the Limit States
Mpkzone = 1.1*Fy*p*tf^2/4;

%Mpbline = 1.1*(1-dh/p)*Fy*p*tf^2/4;
BY1 = 0.95*Bn;
BY2 = Bn;
BY3 = Bfract;

%Set the Initial State for Moment K-zone, Interior Bolt and Exterior Bolt
B1s = 1;
B2s = 1;
Mks = 1;

%Set the First Incremental Load Value and Initialize Total Load Vector T
T = 0;
DeltaT = 5;
```

```matlab
%Initialize the Displacement Vector
D = 0;
Delta = [];

%Initialize the Load Vector
Load = 0;

%Initialize the Moment at the Kzone
Mkzone = 0;

%Set the Force in the Bolts to be Equal to the Pretension Force
Binterior = 0;
Bexterior = 0;

update = 0;

i = 1;
j = 0;
l = 0;

%Calculate Constants Z,X and V
    Z = 1/(1/K1-0.5*a*(b+c)^2/(E*I));
    X = 1/K2+b^3*Z*a*c^2/(E*I*6*2*E*I)-(a+b)*c^2/(2*E*I)-
(a+b)*(b+c)^2*a*c^2*Z/(4*E*I*E*I)-(fs/(G*A))*b*a*c^2*Z/(2*E*I);
    V = ((a+b)^3/(6*E*I)-
a^3*Z*b^3/(36*(E*I)^2)+a*(a+b+c)^2*Z*b^3/(12*(E*I)^2)+(fs/(G*A))*a*Z*b^3/(6*E*I)
-(a+b)*(a+b+c)^2/(2*E*I)+(a+b)*(b+c)^2*a^3*Z/(12*(E*I)^2)-
(a+b)*(b+c)^2*a*(a+b+c)^2*Z/(4*(E*I)^2)-(fs/(G*A))*(a*Z/(E*I))*(a+b)*(b+c)^2*0.5-
(fs/(G*A))*(a+b)+(fs*a^3*b*Z)/(G*A*6*E*I)-(fs*b*Z*a*(a+b+c)^2)/(G*A*2*E*I)-
(fs/(G*A))^2*b*a*Z);

%Calculate the Prying Force Q (Q=Qint+Qext) (kips)
DeltaQ = DeltaT/(a^3*Z/(6*E*I)-a*(a+b+c)^2*Z/(2*E*I)+V*Z*(a*c^2)/(2*E*I*X)-
fs*a*Z/(G*A)-1+V/X);

%Calculate the Force in the Interior and Exterior Bolt
DeltaBinterior = V*DeltaQ/X;

DeltaBexterior = (DeltaQ*a^3/(6*E*I)-
0.5*DeltaQ*a*(a+b+c)^2/(E*I)+0.5*DeltaBinterior*a*c^2/(E*I)-
(fs/(G*A))*DeltaQ*a)*Z;

%Calculate the Moment at the K-zone
```

```matlab
DeltaMkzone = DeltaT*(b+c)-DeltaBinterior*b-DeltaQ*a;

%Set the Termination Condition to be the Interior Bolt Fracture
while(Binterior<Bfract)

%Calculate T that Causes Yielding of the Kzone

ifMks == 1
Tk = 1000;
    Z = 1/(1/K1-0.5*a*(b+c)^2/(E*I));
    X = 1/K2+b^3*Z*a*c^2/(E*I*6*2*E*I)-(a+b)*c^2/(2*E*I)-
(a+b)*(b+c)^2*a*c^2*Z/(4*E*I*E*I)-(fs/(G*A))*b*a*c^2*Z/(2*E*I);
    V = ((a+b)^3/(6*E*I)-
a^3*Z*b^3/(36*(E*I)^2)+a*(a+b+c)^2*Z*b^3/(12*(E*I)^2)+(fs/(G*A))*a*Z*b^3/(6*E*I)
-(a+b)*(a+b+c)^2/(2*E*I)+(a+b)*(b+c)^2*a^3*Z/(12*(E*I)^2)-
(a+b)*(b+c)^2*a*(a+b+c)^2*Z/(4*(E*I)^2)-(fs/(G*A))*(a*Z/(E*I))*(a+b)*(b+c)^2*0.5-
(fs/(G*A))*(a+b)+(fs*a^3*b*Z)/(G*A*6*E*I)-(fs*b*Z*a*(a+b+c)^2)/(G*A*2*E*I)-
(fs/(G*A))^2*b*a*Z);
DeltaMkzone = 1000;

while((DeltaMkzone-((2/3)*Mpkzone-Mkzone))>0.001)
if(DeltaMkzone<((2/3)*Mpkzone-Mkzone))
        Tk = Tk*1.0001;
elseif(DeltaMkzone>((2/3)*Mpkzone-Mkzone))
        Tk = Tk*0.9999;
end

DeltaQ = Tk/(a^3*Z/(6*E*I)-a*(a+b+c)^2*Z/(2*E*I)+V*Z*(a*c^2)/(2*E*I*X)-
fs*a*Z/(G*A)-1+V/X);

DeltaBinterior = V*DeltaQ/X;

DeltaBexterior = (DeltaQ*a^3/(6*E*I)-
0.5*DeltaQ*a*(a+b+c)^2/(E*I)+0.5*DeltaBinterior*a*c^2/(E*I)-
(fs/(G*A))*DeltaQ*a)*Z;

DeltaMkzone = Tk*(b+c)-DeltaBinterior*b-DeltaQ*a;
end

%Note that the equations below should be adjusted to include for partial yielding
elseifMks == 2
Tk = 1000;
    Z = 1/(1/K1-0.5*a*(b+c)^2/(E*I));
```

```matlab
    X = 1/K2+b^3*Z*a*c^2/(E*I*6*2*E*I)-(a+b)*c^2/(2*E*I)-
(a+b)*(b+c)^2*a*c^2*Z/(4*E*I*E*I)-(fs/(G*A))*b*a*c^2*Z/(2*E*I);
    V = ((a+b)^3/(6*E*I)-
a^3*Z*b^3/(36*(E*I)^2)+a*(a+b+c)^2*Z*b^3/(12*(E*I)^2)+(fs/(G*A))*a*Z*b^3/(6*E*I)
-(a+b)*(a+b+c)^2/(2*E*I)+(a+b)*(b+c)^2*a^3*Z/(12*(E*I)^2)-
(a+b)*(b+c)^2*a*(a+b+c)^2*Z/(4*(E*I)^2)-(fs/(G*A))*(a*Z/(E*I))*(a+b)*(b+c)^2*0.5-
(fs/(G*A))*(a+b)+(fs*a^3*b*Z)/(G*A*6*E*I)-(fs*b*Z*a*(a+b+c)^2)/(G*A*2*E*I)-
(fs/(G*A))^2*b*a*Z);
DeltaMkzone = 1000;

while(DeltaMkzone-(Mpkzone-Mkzone)>0.001)
if(DeltaMkzone<(Mpkzone-Mkzone))
        Tk = Tk*1.0001;
elseif(DeltaMkzone>(Mpkzone-Mkzone))
        Tk = Tk*0.9999;
end

DeltaQ = Tk/(a^3*Z/(6*E*I)-a*(a+b+c)^2*Z/(2*E*I)+V*Z*(a*c^2)/(2*E*I*X)-
fs*a*Z/(G*A)-1+V/X);

DeltaBinterior = V*DeltaQ/X;

DeltaBexterior = (DeltaQ*a^3/(6*E*I)-
0.5*DeltaQ*a*(a+b+c)^2/(E*I)+0.5*DeltaBinterior*a*c^2/(E*I)-
(fs/(G*A))*DeltaQ*a)*Z;

DeltaMkzone = Tk*(b+c)-DeltaBinterior*b-DeltaQ*a;
end
end

%Set the Limit State of the Interior Bolt
if B1s == 1
   B1Limit = BY1;
elseif B1s == 2
   B1Limit = BY2;
elseif B1s == 3;
   B1Limit = BY3;
end

%Calculate T that Causes Yielding of the Interior Bolt
ifMks == 1 | Mks == 2
   TB1 = 1000;
   Z = 1/(1/K1-0.5*a*(b+c)^2/(E*I));
```

```matlab
    X = 1/K2+b^3*Z*a*c^2/(E*I*6*2*E*I)-(a+b)*c^2/(2*E*I)-
(a+b)*(b+c)^2*a*c^2*Z/(4*E*I*E*I)-(fs/(G*A))*b*a*c^2*Z/(2*E*I);
    V = ((a+b)^3/(6*E*I)-
a^3*Z*b^3/(36*(E*I)^2)+a*(a+b+c)^2*Z*b^3/(12*(E*I)^2)+(fs/(G*A))*a*Z*b^3/(6*E*I)
-(a+b)*(a+b+c)^2/(2*E*I)+(a+b)*(b+c)^2*a^3*Z/(12*(E*I)^2)-
(a+b)*(b+c)^2*a*(a+b+c)^2*Z/(4*(E*I)^2)-(fs/(G*A))*(a*Z/(E*I))*(a+b)*(b+c)^2*0.5-
(fs/(G*A))*(a+b)+(fs*a^3*b*Z)/(G*A*6*E*I)-(fs*b*Z*a*(a+b+c)^2)/(G*A*2*E*I)-
(fs/(G*A))^2*b*a*Z);
DeltaBinterior = 1000;

while(DeltaBinterior-(B1Limit-Binterior)>0.001)
if(DeltaBinterior<(B1Limit-Binterior))
        TB1 = TB1*1.001;
elseif(DeltaBinterior>(B1Limit-Binterior))
        TB1 = TB1*0.999;
end

DeltaQ = TB1/(a^3*Z/(6*E*I)-a*(a+b+c)^2*Z/(2*E*I)+V*Z*(a*c^2)/(2*E*I*X)-
fs*a*Z/(G*A)-1+V/X);

DeltaBinterior = V*DeltaQ/X;
end
else
TB1 = 1000;
    R = (a+b)/(K1*a)-b^3/(6*E*I)+(fs*b)/(G*A);
    S = -a/(b*K2*R)-(a+b)^3/(6*E*I*R)+a^2*(a+b)/(6*E*I*R)-2;
DeltaBinterior = 1000;

while(DeltaBinterior-(B1Limit-Binterior)>0.001)
if(DeltaBinterior<(B1Limit-Binterior))
        TB1 = TB1*1.0001;
elseif(DeltaBinterior>(B1Limit-Binterior))
        TB1 = TB1*0.9999;
end

DeltaQ = TB1*(1-(b+c)/(b*K2*R)-(b+c)/b)*(1/S);

DeltaBinterior = TB1*(b+c)/b-DeltaQ*a/b;
end
end

%Set the Limit State of the Exterior Bolt
if B2s == 1
    B2Limit = BY1;
```

58

```matlab
elseif B2s == 2
    B2Limit = BY2;
elseif B2s == 3;
    B2Limit = BY3;
end

%Calculate T that Causes Yielding of the Exterior Bolt
ifMks == 1 | Mks == 2
    TB2 = 1000;
DeltaBexterior = 1000;

while(DeltaBexterior-(B2Limit-Bexterior)>0.001)
if(DeltaBexterior<(B2Limit-Bexterior))
        TB2 = TB2*1.0001;
elseif(DeltaBexterior>(B2Limit-Bexterior))
        TB2 = TB2*0.9999;
end

DeltaQ = TB2/(a^3*Z/(6*E*I)-a*(a+b+c)^2*Z/(2*E*I)+V*Z*(a*c^2)/(2*E*I*X)-
fs*a*Z/(G*A)-1+V/X);

DeltaBinterior = V*DeltaQ/X;

DeltaBexterior = (DeltaQ*a^3/(6*E*I)-
0.5*DeltaQ*a*(a+b+c)^2/(E*I)+0.5*DeltaBinterior*a*c^2/(E*I)-
(fs/(G*A))*DeltaQ*a)*Z;
end
else
    TB2 = 1000;
    R = (a+b)/(K1*a)-b^3/(6*E*I)+(fs*b)/(G*A);
    S = -a/(b*K2*R)-(a+b)^3/(6*E*I*R)+a^2*(a+b)/(6*E*I*R)-2;
DeltaBexterior = 1000;

while(DeltaBexterior-(B2Limit-Bexterior)>0.001)
if(DeltaBexterior<(B2Limit-Bexterior))
        TB2 = TB2*1.0001;
elseif(DeltaBexterior>(B2Limit-Bexterior))
        TB2 = TB2*0.99999;
end

DeltaQ = TB2*(1-(b+c)/(b*K2*R)-(b+c)/b)*(1/S);

DeltaBinterior = TB2*(b+c)/b-DeltaQ*a/b;
```

```
DeltaBexterior = (DeltaBinterior/K2-DeltaQ*(a+b)^3/(6*E*I)-
fs*DeltaQ*(a+b)/(G*A)+DeltaQ*a^2*(a+b)/(6*E*I)+fs*DeltaQ*(a+b)/(G*A))/R;
end
end

%Determine the Value of the Stiffness at the Current State
%Case of 1.5 in. thick column flange
ifMks == 1 & B1s == 1 & B2s == 1
    K = Ke1;
elseifMks == 2 & B1s == 1 & B2s == 1
    K = Ke2;
elseifMks>= 3 & B1s == 1 & B2s == 1
    K = Ke3;
elseifMks>= 3 & B1s == 2 & B2s == 1
    K = Ke4;
elseifMks>= 3 & B1s == 3 & B2s == 1
    K = Ke5;
elseifMks>= 3 & B1s == 3 & B2s == 2
    K = Ke6;
elseifMks>= 3 & B1s == 3 & B2s == 3
    K = Ke7;
end

% %Case of 2.25 in. thick column flange
%    if Mks == 1 & B1s == 1 & B2s == 1
%       K = Ke1;
%    elseifMks == 1 & B1s == 2 & B2s == 1
%       K = Ke2;
%    elseifMks == 2 & B1s == 2 & B2s == 1
%       K = Ke3;
%    elseifMks == 2 & B1s == 3 & B2s == 1
%       K = Ke4;
%    elseifMks == 2 & B1s == 3 & B2s == 2
%       K = Ke5;
%    elseifMks == 3 & B1s == 3 & B2s == 2
%       K = Ke6;
%    elseifMks == 3 & B1s == 3 & B2s == 3
%       K = Ke7;
%    end

%Update the Status of Each Limit State
ifTk<TB1 &Tk<TB2 &Mks == 1
DeltaT = Tk;
elseif Tk<TB1 & Tk<TB2 & Mks == 2
```

```matlab
    DeltaT = Tk;
elseif TB1<Tk & TB1<TB2
    DeltaT = TB1;
elseif TB2<Tk & TB2<TB1
DeltaT = TB2;
end

%Calculate the Displacement
DeltaD = (DeltaT)/K;

D = D+DeltaD;

Delta = [Delta D];

%Update the Load Vector
    Load = [Load (Load(i)+DeltaT)];

i = i+1;

ifMks == 1 | Mks == 2
%Recompute Constants Used in the Model for the Current Load Step
    Z = 1/(1/K1-0.5*a*(b+c)^2/(E*I));
    X = 1/K2+b^3*Z*a*c^2/(E*I*6*2*E*I)-(a+b)*c^2/(2*E*I)-
(a+b)*(b+c)^2*a*c^2*Z/(4*E*I*E*I)-(fs/(G*A))*b*a*c^2*Z/(2*E*I);
    V = ((a+b)^3/(6*E*I)-
a^3*Z*b^3/(36*(E*I)^2)+a*(a+b+c)^2*Z*b^3/(12*(E*I)^2)+(fs/(G*A))*a*Z*b^3/(6*E*I)
-(a+b)*(a+b+c)^2/(2*E*I)+(a+b)*(b+c)^2*a^3*Z/(12*(E*I)^2)-
(a+b)*(b+c)^2*a*(a+b+c)^2*Z/(4*(E*I)^2)-(fs/(G*A))*(a*Z/(E*I))*(a+b)*(b+c)^2*0.5-
(fs/(G*A))*(a+b)+(fs*a^3*b*Z)/(G*A*6*E*I)-(fs*b*Z*a*(a+b+c)^2)/(G*A*2*E*I)-
(fs/(G*A))^2*b*a*Z);

%Calculate the Prying Force Q (Q=Qint+Qext) (kips)
DeltaQ = (DeltaT)/(a^3*Z/(6*E*I)-a*(a+b+c)^2*Z/(2*E*I)+V*Z*(a*c^2)/(2*E*I*X)-
fs*a*Z/(G*A)-1+V/X);

%Calculate the Force in the Interior and Exterior Bolt
DeltaBinterior = V*DeltaQ/X;
DeltaBexterior = (DeltaQ*a^3/(6*E*I)-
0.5*DeltaQ*a*(a+b+c)^2/(E*I)+0.5*DeltaBinterior*a*c^2/(E*I)-
(fs/(G*A))*DeltaQ*a)*Z;

%Calculate the Moment at the K-zone
DeltaMkzone = (DeltaT)*(b+c)-DeltaBinterior*b-DeltaQ*a;
```

```matlab
%Update the Value of the Force in the Bolts and the Moment at the Kzone
Binterior = DeltaBinterior+Binterior;
    Bexterior = DeltaBexterior+Bexterior;
Mkzone = Mkzone+DeltaMkzone;

else
%Recompute Constants Used in the Model for the Current Load Step
    R = (a+b)/(K1*a)-b^3/(6*E*I)+(fs*b)/(G*A);
    S = -a/(b*K2*R)-(a+b)^3/(6*E*I*R)+a^2*(a+b)/(6*E*I*R)-2;

%Calculate the Prying Force Q (Q=Qint+Qext) (kips)
DeltaQ = (DeltaT)*(1-(b+c)/(b*K2*R)-(b+c)/b)*(1/S);

%Calculate the Force in the Interior and Exterior Bolt
DeltaBinterior = (DeltaT)*(b+c)/b-DeltaQ*a/b;

    DeltaBexterior = (DeltaBinterior/K2-DeltaQ*(a+b)^3/(6*E*I)-
fs*DeltaQ*(a+b)/(G*A)+DeltaQ*a^2*(a+b)/(6*E*I)+fs*DeltaQ*(a+b)/(G*A))/R;

%Update the Value of the Force in the Bolts and the Moment at the Kzone
Binterior = DeltaBinterior+Binterior;
    Bexterior = DeltaBexterior+Bexterior;

end

%Update the Status of Each Limit State
ifTk<TB1 &Tk<TB2 &Mks == 1
Mks = Mks+1;
elseifTk<TB1 &Tk<TB2 &Mks == 2
Mks = Mks+1;
Tk = 100000;
elseif TB1<Tk& TB1<TB2
    B1s = B1s+1;
    j = j+1;
    K2 = k2(j);
elseif TB2<Tk& TB2<TB1
    B2s = B2s+1;
    l = l+1;
    K1 = k1(l);
end

%Increase the Load Step
DeltaT = 20;
```

```
end
Delta
4*Load
end
```

II. REFERRED PUBLICATIONS

1. Hantouche E, Abboud N. Stiffness modeling of bolted thick built-up T-stub connections including secondary prying effect. J Constr Steel Res 2014;95:279-89.

BIBLIOGRAPHY

[1] Coehlo A, Bijlaard F, Gresnigt N, Da Silva L. Experimental assessment of the behavior of bolted T-stub connections made up of welded plates. J Constr Steel Res 2004;60(2):269–311.

[2] Hantouche E, Rassati G, Kukreti A, Swanson J. Built-up T-stub connections for moment resisting frames: experimental and finite element investigation for prequalification. Eng Struct 2012;43:139–48.

[3] Piluso V, Rizzano G. Experimental analysis and modeling of bolted T-stubs under cyclic loads. J Constr Steel Res 2008;64(6):1007–14.

[4] Piluso V, Faella C, Rizzano G. Ultimate behavior of bolted T-stubs II: model validation. J Struct Eng ASCE 2001;127(6):694–704.

[5] Takhirov S, Popov E. Bolted large seismic steel beam-to-column connections Part 1: experimental study. Eng Struct 2002;24(12):1523–34.

[6] Roddis K, Blass D. Tensile capacity of single-angle shear connections considering prying action. J Struct Eng ASCE 2013;139:504–14.

[7] Coehlo A, Da Silva L, Bijlaard F. Finite element modeling of the nonlinear behavior of bolted T-stub connections. J Struct Eng ASCE 2006;132(6):918–28.

[8] Hantouche E, Kukreti A, Rassati G. Investigation of secondary prying in thick built-up T-stub connections using nonlinear finite element modeling. Eng Struct 2012;36:113–22.

[9] Swanson J, Kokan D, Leon R. Advanced finite element modeling of bolted T-stub connection components. J Constr Steel Res 2002;58(5):1015–31.

[10] Hantouche E, Kukreti A, Rassati G, Swanson J. Modified stiffness model for thick flange in built-up T-stub connections. J Constr Steel Res 2013;81:76–85.

[11] Hu J, Leon R, Park T. Mechanical modeling of bolted T-stub connections under cyclic loads Part I: stiffness modeling. J Constr Steel Res 2011;67(11):1710–8.

[12] Hu J, Leon R, Park T. Mechanical models for the analysis of bolted T-stub connections under cyclic loads. J Constr Steel Res 2012;78(11):45–7.

[13] Lemonis M, Gantes C. Incremental modeling of T-stub connections. J Mech Mater 2006;1(7):1135–59.

[14] Piluso V, Faella C, Rizzano G. Ultimate behavior of bolted T-stubs I: theoretical model. J Struct Eng ASCE 2001;127(6):686–93.

[15] Swanson J, Leon R. Stiffness modeling of bolted T-stub connection components. J Struct Eng ASCE 2001;127(5):498–505.

[16] Comité Europènne de Normalisation CEN. Eurocode3: Design of steel structures, Part1–8: design of joints and building frames. Brussels (Belguim): ENV 1993-1-8; 2005.

[17] ABAQUS, Dassualt Systems, Pawtucket, RI.2011.

[18] American Institute of Steel Construction AISC. ANSI/AISC 341-05 seismic provisions for structural steel buildings. Chicago (IL): AISC; 2005.

[19] American Institute of Steel Constuction AISC. ANSI/AISC 360–05 load and resistance factor design specification for structural steel buildings. Chicago (IL): AISC; 2005

[20] Piluso V, Rizzano G. Experimental analysis and modeling of bolted T-stubs under cyclic loads. J Constr Steel Res 2008;64:655–69.

[21] Abolmaali A, Kukreti A, Motahari A, Ghassemieh M. Energy dissipation characteristics of semi-rigid connections. J Constr Steel Res 2009;65:1187–97.

[22] Hantouche E, Rassati G, Swanson J. Built-up T-stub connection for special and inter- mediate moment frames. Numerical and experimental testing for prequalification. STESSA 2009 conference; 2009.p. 275–80 [Lehigh (PA)].

[23] Hantouche E. Behavior of thick built-up T-stub connections for moment resisting frames. Ph.D. thesis Ohio: University of Cincinnati; 2011.

[24] Larson P. The design and behavior of bolted beam-column frame connections under cyclical loading. M.S. thesis Austin (TX): University of Texas Austin; 1996.

[25] Smallidge J. Behavior of bolted beam-to-column T-stub connections under cyclic loading. M.S. thesis Atlanta (GA): Georgia Institute of Technology; 1999.

[26] Swanson J. Characterization of the strength, stiffness, and ductility behavior of T-stub connections. Ph.D. thesis Atlanta (GA): Georgia Institute of Technology; 1999.

[27] McManus P, Puckett J. Repairable seismic moment frames with bolted WT connections: part I. Eng J 2011;48(4):265–82.